Hypoxia-inducible-factors differentially contribute to clinical disease and viral replication during RSV infection

Dorothea R. Morris[1,2,3], Yue Qu[3], Aline Haas de Mello[3], Yava L. Jones-Hall[4], Tianshuang Liu[3], Meredith Weglarz[1], Teodora Ivanciuc[3], Roberto P. Garofalo[1,3], Antonella Casola[1,3,*]

[1]Department of Microbiology & Immunology, The University of Texas Medical Branch, Galveston, TX, USA

[2]School of Population & Public Health, The University of Texas Medical Branch, Galveston, TX, USA

[3]Department of Pediatrics, The University of Texas Medical Branch, Galveston, TX, USA

[4]School of Veterinary Medicine and Biomedical Science, Texas A&M University, College Station, TX, USA

*** Correspondence:**
Antonella Casola
ancasola@utmb.edu

Keywords: RSV, respiratory syncytial virus, hypoxia-inducible-factors, HIF-1a, HIF-2a, PX478, PT2385

1 Abstract

Hypoxia-inducible-factors (HIF) are transcription factors that regulate cellular adaptation to hypoxic conditions, enabling cells to survive in low-oxygen environments. Viruses have evolved to activate this pathway to promote successful viral infection, therefore modulation of HIFs could represent a novel antiviral strategy. In previous *in vitro* studies, we found that respiratory syncytial virus (RSV), a leading cause of respiratory illness, stabilizes HIFs under normoxic conditions, with inhibition of HIF-1α resulting in reduced viral replication. Despite several HIF modulating compounds being tested/approved for use in other non-infectious models, little is known about their efficacy against respiratory viruses using relevant animal models. This study aimed to characterize the disease modulating properties and antiviral potential of HIF-1α (PX478) and HIF-2α (PT2385) inhibitors in RSV-infected BALB/c mice. We found that inhibition of HIF-1α worsen clinical disease parameters,

25 while simultaneously improving lung inflammation and airway function. Additionally, blocking HIF-
26 1α resulted in significantly reduced viral titer at early and peak time points of RSV replication. In
27 contrast, inhibition of HIF-2α was associated with improved clinical parameters, with no changes in
28 airway function, enhanced immune responses and reduced early and peak lung viral replication.
29 Analysis of lung cells found significant modification in the T-cell compartment that correlated with
30 changes in lung pathology and viral titers in response to each HIF inhibitor administration. This study
31 underscores the differential roles of HIF proteins in RSV infection and highlights the need for further
32 characterization of the compounds that are currently in use or under therapeutic consideration.

33 **2 Introduction**

34 Respiratory syncytial virus (RSV) is a prominent cause of respiratory infections among infants,
35 young children, and the elderly. Each year, there are an estimated 33 million infections and 150,000
36 deaths [1]. Infection with RSV often results in damage to the airways and a dysregulated immune
37 response that contributes to the development of bronchiolitis and pneumonia. Although prophylactic
38 treatment and vaccines licensed for use in pregnant women and elderly patients are available, there are
39 no therapeutic agents licensed for the treatment of RSV infection [2-4]. Furthering our understanding
40 of the pathology of RSV is important to protecting these vulnerable populations.

41 As an obligate intracellular pathogen, viruses rely on host-cell machinery to establish productive
42 infections. Many viruses have been shown to modify cellular metabolism to achieve virion assembly
43 by increasing sources of energy and generating pools of free nucleotides, amino acids, lipid materials,
44 and glycoproteins [5]. One mechanism frequently associated with this is the manipulation of the
45 hypoxia-inducible-factor (HIF) pathway. As the gatekeeper to a diverse biological network, the use of
46 the HIF pathway allows many viruses to create a cellular environment that favors viral replication,
47 persistence, and immune evasion. The manipulation of this pathway has been observed with several
48 DNA and RNA viruses, even under oxygen-rich conditions [6, 7]. The significance of HIF in cancer

49 pathology has led much of the existing literature to focus on viruses known to induce tumor formation
50 as part of their pathogenic mechanism [6, 7]. Surprisingly, limited research has explored the clinical
51 manifestations and pathological contributions of HIFs to viral respiratory infections [6-9].

52 HIFs are transcription factors that regulate the expression of a wide range of target genes in
53 response to low oxygen levels [10]. These target genes have crucial roles in diverse biological
54 processes, enabling cells to adapt and survive under hypoxic conditions. The HIF complex is a
55 heterodimer consisting of an inducible α subunit (HIF-1α, HIF-2α, or HIF-3α) and a constitutively
56 expressed β subunit (HIF-1β) [11]. While there is overlap in their functionality, the HIF-α isoforms
57 also exhibit distinct transcriptional regulation in response to hypoxia and disease states [12-14]. HIF-
58 1α is the most extensively studied isoform of the HIF family. Expressed in nearly all cell types, HIF-
59 1α is the master regulator of cellular and systemic responses to hypoxia. Genes activated by HIF-1α
60 modify a broad range of processes including energy metabolism, angiogenesis, epithelial-
61 mesenchymal transition (EMT), and immune cell regulation [12, 14]. HIF-2α, though not as thoroughly
62 described as HIF-1, has been shown to exhibit a more limited distribution; predominately expressed in
63 specific organs such as the kidney, liver, and lung. Genes upregulated by HIF-2α in models of cancer
64 and of non-infectious tissue repair are primarily involved in erythropoiesis, vascular development, and
65 iron metabolism [14]. HIF-3α is the most recent of the HIF isoforms to be identified. Because of this,
66 the precise distribution and function of HIF-3α is still being investigated.

67 Our laboratory recently found that RSV stabilizes both HIF-1α and HIF-2α in primary small
68 airway epithelial cells and diverts core metabolic activity towards the glycolytic pathway in a HIF-1α
69 dependent manner [15]. Inhibition of HIF-1α, but not HIF-2α, was associated with reduced viral
70 replication. Given the multiple roles of HIFs in both the epithelial and immune compartments, we
71 investigated their involvement in RSV lung disease and pathology by utilizing established inhibitors

72 of HIF-1α (PX478) and HIF-2α (PT2385) in a BALB/c mouse model. Our results underscore the
73 distinct functionality of the individual HIF-α subunits in the development of RSV pathogenesis and
74 indicate the importance of testing HIF therapeutics approved for conditions such as cancer in complex
75 viral respiratory infection biological models for potential benefits, but also unwanted side effects.

76 **3 Materials and methods**

77 **3.1 Animal experiments**

78 Female, 8 to 10-week-old BALB/c mice were purchased from Envigo (Indianapolis, IN, USA).
79 Mice received either PX478 or PT2385 (HY-10231 and HY-12867, MedChemExpress, Monmouth
80 Junction, NJ, USA) by oral gavage at a dose of 20 or 50 mg/kg, respectively. PX478 was dissolved in
81 PBS, while PT2385 was dissolved in 10% DMSO + 90% Corn Oil (CO). For anti-HIF1α, PX478
82 treated mice were separated into three groups. The first received PBS as the control group. The second
83 received PX478 every 24 h for 10 days (PXQD). The third group received PX478 every 48 h for 10
84 days (PXQAD). For anti-HIF2α, mice received either CO or PT2385 every 24 h for 10 days. Within
85 15 minutes of the first treatment, mice were anesthetized and intranasally (IN) inoculated with 50μL
86 of either PBS or RSV Long Strain at a dose of $5x10^6$ plaque forming units (PFU). Preparation of RSV
87 Long Strain (ATCC, Manassas, VA, USA) was done as described previously [16]. All mice were
88 monitored over the 10-day infection period for changes in bodyweight loss and clinical illness score
89 on a 0-to-5 grading scale (0 = healthy, 1 = barely ruffled fur, 2 = ruffled fur but active, 3 = ruffled fur
90 and inactive, 4 = ruffled fur, inactive and hunched, 5 = dead). All care and procedures involving mice
91 in this study were completed in accordance with the recommendations in the *Guide for the Care and*
92 *Use of Laboratory Animals* of the National Institutes of Health and the UTMB institutional guidelines
93 for animal care. The Institutional Animal Care and Use Committee (IACUC) of UTMB approved these
94 animal studies under protocol 9001002.

95

96 **3.2 RNA extraction and reverse transcription-quantitative PCR (RT-qPCR)**

97 Lung tissue was homogenized in TRIzol reagent (15596018; Thermo Fisher Scientific, Waltham,
98 MA, USA) and the RNA was isolated using a combination of TRIzol-based method and the RNeasy
99 Mini Kit (74104; Qiagen, Hilden, Germany). Briefly, after phase separation with chloroform, the top
100 aqueous layer was further processed using the Qiagen RNeasy Mini kit spin columns by following
101 manufacturer's protocol. On-column DNase digestion was performed with the RNase-free DNase set
102 (79254; Qiagen). cDNA synthesis was performed with 1 µg of RNA using iScript Reverse
103 Transcription Supermix (1708841; Bio-Rad Laboratories, Hercules, CA, USA). The cDNA was diluted
104 four times with nuclease-free water, and the qPCR was done using 4 µL of cDNA, pre-mixed probe
105 and primers (TaqMan Gene Expression Assays, Applied Biosystems, Waltham, MA, USA), and
106 TaqMan Universal Master Mix (4440040; Applied Biosystems). The Custom Plus TaqMan RNA
107 Assay (4441114, Applied Biosystems) was used to assess the expression of *RSV N* (Assay ID:
108 ARU66XH). The following mouse TaqMan Gene Expression Assays (4331182, Applied Biosystems)
109 were used: *Hif1α* (Mm00468869_m1), *Pgk1* (Mm00435617_m1), *Hk2* (Mm00443386_m1), *Slc2a1*
110 (Mm00441480_m1), *Serpine1* (Mm00435858_m1), *Epo* (Mm01202755_m1) and *Epas1*
111 (Mm01236112_m1). The Eukaryotic 18S rRNA Endogenous Control (4352930E, Applied
112 Biosystems) was used for normalization. The qPCR assays were run in the Bio-Rad CFX Connect real-
113 time system. The delta-delta Ct method was used to calculate the relative changes in gene expression.

114 **3.3 Bronchoalveolar lavage and viral replication**

115 The BAL fluid was obtained as previously described [17]. A small aliquot was used to determine
116 the total cell count and cellular differentiation of the BAL by cytospin analysis. The remaining BAL
117 fluid was centrifuged, and the supernatants were collected and stored at -80C. To assess viral

118 replication, lungs were collected from mice at days 2, 4, 7, and 10 post-infection (p.i.) to perform
119 plaque assays, as previously described [17].

120 **3.4 Flow cytometry**

121 At days 1, 2, 4 and 7 p.i., mice were euthanized and the whole lung was collected. The tissue was
122 minced and digested with 10mg/mL DNase I (Sigma-Aldrich, St. Louis, MO, USA) and 50mg/mL
123 collagenase IV (Worthington Biochemical, Lakewood, NJ, USA). The tissue was incubated at 37C for
124 30 minutes and then passed through a 70-µm cell strainer in RPMI 1640 medium + 10% FBS (CRPMI)
125 and red blood cells were removed by using Red Blood Cell Lysis Buffer (Sigma-Aldrich, Burlington,
126 MA, USA). TruStain FcX (Biolegend, San Diego, CA, USA) was first used to reduce non-specific
127 binding, followed by Zombie NIR Viability dye. To assess cellular populations of neutrophils, alveolar
128 macrophages, and natural killer (NK) cells at days 1 and 2 p.i. a comprehensive panel of fluorochrome-
129 labeled antibodies was utilized. The antibodies employed included FITC-anti-CD45 (clone 30-F11),
130 BV785-anti-CD11b (clone M1/70), PerCP/Cyanine 5.5-anti-Ly6G (clone 1A8), BUV395-anti-CD11c
131 (clone HL3), PE-Cy7-anti-F4/80 (clone BM8), BV510-anti-MHCII (clone M5/114.15.2), BV711-anti-
132 CD3ε(clone 145-2C11), and PE/Dazzle 594-anti-CD49b (clone DX5). For the analysis of $CD4^+$ and
133 $CD8^+$ T-cell populations at days 4 and 7 p.i. the panel included: FITC-anti-CD45 (clone 30-F11),
134 BV785-anti-CD3 (clone 17A2), AF 700-anti-CD4 (clone GK1.5), BV510-anti-CD8a (clone 53-6.7),
135 PerCP/Cy5.5-anti-CD44 (clone IM7), BV605-anti-CD62L (clone MEL-14), and PE/Cy7-anti-CD69
136 (clone H1.2F3). All antibodies were purchased from Biolegend, Thermo Fisher Scientific, Novus
137 Biologicals, or R&D Systems and titrated prior to use. Data were acquired on a BD FACSymphony
138 A5 SE in the UTMB Flow Cytometry and Cell Sorting Core and analyzed using FlowJo software
139 version 10.9.0 (BD Bioscience, Franklin Lakes, NJ, USA).

140

141 **3.5 Assessment of airway function and lung histopathology**

142 Bronchoconstriction was evaluated by measuring Penh values in unrestrained mice using whole-
143 body barometric plethysmography (Buxco, Troy, NY, USA) as previously described [18]. Total protein
144 was measured using BioRad Total Protein Dye (Bio-Rad Laboratories, Hercules, CA, USA). For
145 histology, the left lung was collected from mice at days 4, 7, and 10. The tissue was fixed in 10%
146 neutral buffered formalin and subjected to paraffin embedding. Sections were cut and stained with
147 H&E and evaluated by a board-certified pathologist with expertise in mouse lung (Y.L.J.-H).
148 Assessment of the tissue was done as previously described [19].

149 **3.6 Statistical analysis**

150 Statistical analyses were performed using a two-way mixed ANOVA or an unpaired student's
151 t-test as appropriate. Analyses were done using GraphPad Prism 9.5.1 (GraphPad Software, Inc., San
152 Diego, CA, USA). Results are expressed as mean ± SEM and $p \leq 0.05$ value was selected to indicate
153 significance.

154 **4 Results**

155 **4.1 Effect of PX478 administration on RSV infection associated disease parameters and viral**
156 **replication.**

157 To investigating the role of HIF-1α in RSV disease, groups of BALB/c mice were initially
158 administered PX478 at a dose of 20 mg/kg by oral gavage every 24 h (PXQD) over the 10-day infection
159 period (Fig. S1A). Shortly after the first dose of PX478, mice were anesthetized and intranasally (IN)
160 infected with RSV at a dose of $5x10^6$ PFU. We found that PXQD treatment was associated with
161 worsening body weight and illness score, characterized by an inability to regain weight regardless of
162 infection status (Fig. S1B, S1C).

163 To assess airway function during RSV infection, we measured bronchoconstriction using whole-
164 body plethysmography, as previously described [17]. Uninfected mice that received PX478 showed no
165 significant alterations of Penh values at any timepoint tested, compared to the PBS/PBS control group.
166 RSV infected PX478-treated mice showed significant improvement in Penh at days 1, 5, and 6 p.i.,
167 with values comparable to the PBS/PBS control mice throughout the disease course (Fig. S1D).

168 We next measured total protein level in the BAL fluid as an indicator of epithelial damage.
169 PX478 treatment did not alter BAL protein levels in uninfected mice, while RSV infected PX478-
170 treated mice showed significant improvements in total protein at day 4 p.i., compared to the RSV/PBS
171 control mice (Fig. S1E).

172 To assess the effect of PX478 treatment on viral replication, we performed plaque assays at early
173 and peak timepoints of day 2 and 4 p.i.. We found that PX478 treatment significantly reduced
174 replication of days 2 and 4 p.i., when compared to the RSV/PBS control mice. However, RSV
175 replication in RSV PX478-treated mice persisted through day 7 p.i., a timepoint when RSV/PBS
176 control mice had achieved viral clearance, with some mice having detectable replication in the lung
177 tissue as late as day 10 p.i. (Fig. S1F).

178 To improve the toxicity observed on body weight loss and illness in the PBS/PXQD treated mice,
179 we tested lower doses of the compound (5 to 15 mg/kg) for changes in body weight and viral
180 replication. Following the same treatment schedule, we found bodyweight to be improved for some of
181 the doses in PBS mice treated with PX478, but none of the RSV mice treated with PX478 had
182 comparable antiviral activity (data not shown). The administration of PX478 at 20 mg/kg was then
183 changed to every 48 h (PXQAD) over the 10-day infection period (Fig. 1A). Uninfected mice that
184 received the compound on alternate days no longer exhibited substantial weight-loss or heightened
185 illness in comparison to the PBS/PBS control mice. However, RSV infected mice treated with PXQAD
186 continued to demonstrate significantly worse body weight-loss and illness score in comparison to the
187 RSV/PBS mice, although these mice showed signs of recovery at the later stages of the disease course
188 (Fig. 1B, 1C).

189 Lung function was assessed by measuring bronchoconstriction (Penh) and BAL total protein
190 levels. RSV infected mice that received PXQAD had significant improvements in Penh at days 1, 5,
191 and 6 p.i., with values comparable to the PBS/PBS control mice throughout the disease course (Fig.
192 1D). RSV/PXQAD mice also had significant improvement in BAL total protein level at day 4 p.i. as
193 compared to the RSV/PBS control mice (Fig. 1E).

194 To assess the effect of PXQAD treatment on viral replication, we performed plaque assays at
195 early and peak timepoints of day 2 and 4 p.i, as well as days 7 and 10 p.i. to assess viral clearance.
196 RSV/PXQAD mice showed significantly reduced RSV replication at day 4 p.i., with no significant
197 difference in viral clearance at days 7 and 10 p.i. when compared to the RSV/PBS group (Fig. 1F). The
198 change in peak RSV replication was further supported by reductions in the RSV *N* gene by RT-qPCR
199 at day 4 p.i. (Fig. 1G). All subsequent experiment described below were then performed using the
200 PXQAD treatment protocol.

201

202 **4.2 Effect of PX478 administration on RSV-induced HIF-1α target genes.**

203 To confirm inhibition of RSV-induced HIF-1α activation by PX478 treatment, we analyze the
204 expression of *Hif1α* and the HIF-1α-target genes phosphoglycerate kinase 1 (*Pgk1*), hexokinase 2
205 (*Hk2*), and solute carrier family 2 (facilitated glucose transporter) member 1 (*Slc2a1*), at day 2 p.i. in
206 lungs of mice untreated or treated with the compound (Fig. 2). RSV infection resulted in upregulation
207 of HIF-1α and HIF-1α-target genes, which was significantly reduced by PX478 treatment. Specificity
208 of PX478 was determined by assessment of the HIF-2α–dependent genes erythropoietin (*Epo*) and
209 *Serpine1*. *Epo* was not detectable in the lung tissue of any mice. RSV infection induced the expression
210 of *Serpine1*, which was not changed by PX478 treatment, indicating specificity of the compound.

211 **4.3 Inhibition of HIF-1α leads to reduced immune responses following RSV infection.**

212 The immune response to an RSV infection plays a key role in determining disease severity and
213 the control of RSV replication [20]. To understand the impact of HIF-1α inhibition on the immune
214 response to RSV, we first evaluated the cellular composition of the BAL fluid. Uninfected mice that
215 received PXQAD showed no significant changes of BAL cellular composition as compared to the
216 PBS/PBS control mice (Fig. 3A-D). On the other hand, RSV infected mice that received the compound
217 demonstrated significant reductions in the number of total cells present in the BAL (Fig. 3A),
218 specifically in the number of lymphocytes (Fig. 3B) and macrophages (Fig. 3C) at all time points tested,
219 compared to RSV/PBS mice. Neutrophil cell counts were also significantly reduced at day 2 p.i. but
220 remained similar to the RSV/PBS control mice at all other time points (Fig. 3D). Together, these data
221 suggest HIF-1α is important for the recruitment of immune cells within the airway space.

222 $CD4^+$ and $CD8^+$ T-cells play a fundamental role in controlling RSV replication and clearance
223 within the host [20-22]. With reduced lymphocyte numbers in the BAL and the complex outcome to
224 viral replication (prolonged viral replication in the PXQD treatment schedule), we next wanted to
225 assess the impact of HIF-1α inhibition on the T-cell population within the lung tissue. To do so, flow

226 cytometry analysis was performed using whole lung tissue at days 4 and 7 p.i. as depicted in Fig. S2.
227 RSV infected mice treated with PXQAD demonstrated a significant reduction of total leukocytes (Fig.
228 4A), $CD4^+$ (Fig. 4B) and $CD8^+$ (Fig. 4C) T-cells present in the lungs at days 4 and 7 p.i., compared to
229 the RSV/PBS control mice. We then further examined $CD4^+$ T-cell subpopulations including naïve,
230 effector, and active cells. We found the absolute cell numbers for all three $CD4^+$ subpopulations to be
231 significantly reduced at day 4 p.i. (Fig. 4D and Table S1). In accordance, the percentage of effector
232 and active $CD4^+$ cells were decreased while the percent of naïve $CD4^+$ cells increased as compared to
233 the RSV/PBS control mice (Table S1). At day 7 p.i., the absolute cell counts of effector $CD4^+$ T-cells
234 remained significantly reduced in the lung tissue of RSV/PXQAD mice. The absolute cell counts for
235 naïve and active $CD4^+$ T-cells as well as the percent change for all three $CD4^+$ subpopulations were
236 comparable to the RSV/PBS control mice at day 7 p.i. (Fig. 4D and Table S1).

237 We similarly assessed $CD8^+$ subpopulations including naïve, effector, and active cells. At day 4
238 p.i., RSV/PXQAD mice had a trend for reduced absolute cell number of effector cells and significant
239 reductions in the absolute cell numbers for the naïve and active $CD8^+$ subpopulations as compared to
240 the RSV/PBS control mice (Fig. 4E and Table S1). In accordance, the percentage of effector and active
241 $CD8^+$ cells were decreased while the percent of naïve $CD8^+$ cells increased (Table S1). At day 7 p.i.,
242 the absolute cell counts of effector and active $CD8^+$ T-cells were significantly reduced (Fig. 4E).
243 Similarly, the percent change of effector $CD8^+$ cells was reduced, while the percent of naïve and active
244 $CD8^+$ T-cells remained comparable to the RSV/PBS control mice (Table S1). Collectively, these data
245 indicate that HIF-1α plays an important role in regulating T-cell responses during RSV infection by
246 modulating T-cell recruitment to the lung and their activation.

247 Last, we assessed the lung tissue of mice that received PXQAD by histopathology. Based on the
248 scoring determined by a board-certified veterinarian with expertise in mouse lung morphology,
249 uninfected mice that received PXQAD remained comparable to the PBS/PBS control mice in all
250 categories and at all timepoints tested. RSV/PXQAD mice demonstrated significant improvements to

251 the total lung score as compared to the RSV/PBS control mice (Fig. 5A). Specifically, perivasculitis
252 (Fig. 5B) and peribronchiolitis (Fig. 5C) were significantly improved at days 4 and 7 p.i. as compared
253 to the RSV/PBS control mice. This finding is consistent with the reduction of immune cells noted in
254 the BAL and lung tissue of these mice. No significant differences in the percent of abnormal lung field
255 (Fig. 5D) or the severity of interstitial pneumonia (Fig. 5E) were appreciated at any time point.
256 Representative images of the lung tissue for RSV/PBS and RSV/PXQAD mice are shown in Fig.6.
257 Collectively, these data suggest HIF-1α to contribute to the worsening of airway function and tissue
258 damage during the acute phase of RSV infection.

259 **4.4 Effect of PT2385 administration on RSV infection associated disease parameters and viral**
260 **replication.**

261 While there is a degree of functional overlap between the HIF-α subunits, they have also been
262 demonstrated to govern a distinct range of biological activities [14]. To better understand the specific
263 role of HIF-2α during RSV infection, mice were administered PT2385 by oral gavage every 24 h at a
264 dose of 50mg/kg (Fig. 7A). Shortly after the first dose, mice were anesthetized and infected with RSV
265 at a dose of $5x10^6$ PFU. Uninfected mice that received PT2385 were found to have similar body weight
266 loss and illness score as the PBS/CO control mice (Fig. 7B-7C). RSV infected mice that received
267 PT2385 demonstrated significant improvements to bodyweight loss at several timepoints over the 10-
268 day disease course as compared to the RSV/CO control mice (Fig. 7B). Interestingly, the illness score
269 in RSV/PT2385 mice was worse at day 4 p.i., but treated animals showed a quicker recovery at later
270 time points of infection when compared to the RSV/CO control mice (Fig. 7C).

271 To assess airway function during RSV infection, we measured bronchoconstriction and BAL
272 total protein levels. Uninfected mice that received PT2385 showed no significant alterations to Penh
273 values at any timepoint tested as compared to the PBS/CO control mice. Similarly, RSV infected mice
274 treated with PT2385 had similar Penh values as the RSV/CO control mice throughout the 10-day

275 disease course (Fig. D). We observed no significant differences in total protein for all mice tested as
276 compared to their respective control groups (Fig. 7E).

277 Assessment of viral replication in the lung tissue, assessed by plaque assay and viral gene
278 expression, showed RSV/PT2385 mice to have reduced RSV replication at early and peak timepoints
279 of days 2 and 4 p.i. (Fig. 7F and 7G). By days 7 and 10 p.i., no replicating virus was detected in
280 RSV/PT2385 mice, indicating successful clearance of RSV from the lung tissue. Collectively, these
281 data suggest HIF-2α contributes to RSV-induced disease and control of viral replication.

282 **4.5 Effect of PT2385 administration on RSV-induced HIF-2α target genes.**

283 To confirm inhibition of RSV-induced HIF-2α activation by PT2385 treatment, we analyze the
284 expression of *Epas1* (HIF-2α) and the HIF-2α-target genes *Serpine1* and *Epo* at day 2 p.i. in lungs of
285 mice untreated or treated with the compound (Fig. 8). There was no change in baseline HIF-2α gene
286 expression (*Epas1*) following RSV infection, different from what we observed for HIF-1α. We
287 confirmed induction of the HIF-2α-target gene *Serpine1*, which was significantly reduced by PT2385
288 treatment. *Epo* was not detectible in the lung tissue of any mice. There was no change in RSV-induced
289 expression of HIF-1α-dependent genes *Hk2, Slc2a1*, and *Pgk1* following treatment, indicating
290 specificity of the compound (Fig. 8).

291 **4.6 Inhibition of HIF-2α leads to increased immune activity in the BAL and lung tissue of**
292 **RSV infected mice.**

293 We had previously demonstrated HIF-2α to be dispensable for the control of RSV replication in
294 human small airway epithelial cell [23]. Given the antiviral outcome in RSV/PT2385 mice, we next
295 wanted to understand the contribution of HIF-2α to the immune response during an RSV infection. We
296 first evaluated the cellular composition of the BAL fluid. Uninfected mice that received PT2385
297 showed no significant difference in BAL cellular composition, compared to the PBS/CO control group
298 (Fig. 9A-D). RSV infected mice that received PT2385 demonstrated a significant increase in the

299 number of total of cells present in the BAL throughout the course of the infection (Fig. 9A), particularly
300 for the number of lymphocytes (Fig. 9B), compared to the PBS/CO control group. Macrophage cell
301 counts were also significantly increased at days 2 and 10 p.i. (Fig. 9C), while neutrophil cell counts
302 remained comparable to the RSV/CO control mice (Fig. 9D).

303 Given the increase in some innate cells in the BAL, we next assessed a few innate immune cells
304 speculated to contribute to RSV antiviral activity by flow cytometry. Whole lung tissue was collected
305 from RSV infected mice treated or not with PT2385 at days 1 and 2 p.i., the peak of innate immune
306 cell activity in RSV infected mice. We assessed the tissue for alveolar macrophages, neutrophils,
307 natural killer (NK), and natural killer T (NKT) cells. We found a significant increase in absolute cell
308 count of neutrophils on day 2 p.i. in the lungs of RSV/PT2385 mice as compared to the RSV/CO
309 control mice (Fig. 10A). Absolute cell counts of alveolar macrophages, NK, and NKT cells were
310 comparable between the two groups (Fig. 10B-D).

311 As with HIF-1α, we next assessed $CD4^+$ and $CD8^+$ T-cell responses by flow cytometry analysis.
312 RSV infected mice treated with PT2385 demonstrated a significant increase of total leukocytes (Fig.
313 11A), $CD4^+$ (Fig. 11B) and $CD8^+$ (Fig. 11C) T-cells in the lung at day 4 p.i.. We further analyzed the
314 $CD4^+$ T-cell subpopulations of naïve, effector, and active T-cells. In RSV/PT2385 mice at day 4 p.i.,
315 we observed an increasing trend in total number of $CD4^+$ naïve cells as well as a significant increase
316 in the absolute number of $CD4^+$ effector and active T-cells as compared to the RSV/CO control mice
317 (Fig. 11D). The percent change at day 4 p.i. was similar amongst all $CD4^+$ T-cell subpopulations when
318 compared to the RSV/CO control mice (Table S2). By day 7 p.i., the absolute cell counts and percent
319 change of all $CD4^+$ T-cells in the RSV/PT2385 were of comparable number to the RSV/CO control
320 mice. For $CD8^+$ T-cell subpopulations, we observed a significant increase in absolute number of $CD8^+$
321 naïve cells at day 4 p.i., while the absolute cell counts for effector and active $CD8^+$ T-cells remained
322 similar to the RSV/CO control mice (Fig. 11E). At day 7 p.i., the absolute number of active $CD8^+$ T-

323 cells was significantly increased, while the naïve and effector $CD8^+$ cells remained comparable to the
324 RSV/CO control mice (Fig. 11E). The percent change was not modified for any $CD8^+$ cells at either
325 timepoint (Table S2). Collectively, these data show that inhibition of HIF-2α results in increased T-
326 cell numbers, which could contribute to better control of RSV replication, resulting in decreased viral
327 titers.

328 Lastly, we assessed the lung tissue of mice that received PT2385 by histopathology. Uninfected
329 mice that received PT2385 remained comparable to the PBS/CO control mice in all categories and at
330 all time points tested. RSV infected mice treated with PT2385 demonstrated significant improvements
331 at day 10 p.i. in total lung score (Fig. 12A), peribronchiolitis (Fig. 12C), and the severity of interstitial
332 pneumonia (Fig. 12E) as compared to the RSV/CO control mice. The percent abnormal lung field was
333 found to have a trend towards improvement in RSV/PT2385 mice (Fig. 12D). Additionally, there was
334 mild worsening of perivasculitis compared to the RSV/CO control mice (Fig. 12B). Representative
335 images of the lung tissue for RSV/CO and RSV/PT2385 mice are shown in Fig.13. Collectively, these
336 data suggest HIF-2α does not modify airway function but does contribute to worsening lung pathology
337 during the acute phase of RSV infection.

338 **5 Discussion**

339 The pharmacological use of HIF therapeutics has been extensively explored in various models
340 of cancer, autoimmunity, and non-infectious lung damage [7, 22, 23]. While some studies have
341 demonstrated the antiviral potential of HIF inhibitors against respiratory viruses, these findings have
342 been primarily limited to *in vitro* characterizations [8]. Our laboratory has previously shown that
343 RSV infection results in the stabilization of both HIF-1α and HIF-2α. Through pharmacological
344 inhibition of HIF, we also demonstrate the stabilization of HIF-1α, but not HIF-2α, to orchestrate
345 metabolic reprogramming towards glycolysis and for this activity to be important for RSV replication
346 in lung epithelial cells [14]. Given the diverse biological role of HIFs across several cellular

347 compartments, we next wanted to understand the function of these inhibitors in a mouse model of
348 RSV infection. In this study, we aimed to characterize the disease modulating properties and antiviral
349 potential of HIF-1α and -2α inhibitors in a BALB/c mouse model of RSV infection.

350 Our results show that inhibition of HIF-1α worsens clinical disease while concurrently
351 improving aspects of airway function and lung inflammation during RSV infection. In our initial
352 experiments with PX478, when administering the inhibitor every-day (QD), we observed notable
353 weight loss and increased illness in the PBS/PXQD mice compared to the PBS control mice. As there
354 was no difference in any other parameter analyzed, including BAL cells (data not shown), this result
355 suggests that the deteriorating clinical condition in PBS/PXQD mice is likely influenced by a factor
356 other than inflammation or tissue damage. Previous studies investigating the anti-tumor efficacy of
357 PX478 have administered this compound for up to 5 consecutive days, reporting minor weight-loss in
358 the mice during that time [24, 25]. Studies using obese mouse models have noted PX478 to prevent
359 weight gain [26, 27] and a recent investigation has shown the efficacy of PX478 as a potential
360 therapeutic for type-II diabetes [28]. Considering the significant role of HIF-1α in metabolic function
361 and the recent repositioning of PX478 for treatment of type-II diabetes, it is possible that consecutive
362 dosing of PX478 for extended periods of time may lead to appetite suppression. In our model,
363 spacing treatments over 48 h (QAD) ameliorated this effect, resulting in patterns of clinical disease in
364 the PBS/PXQAD mice that resemble previously reported observations. Despite this, RSV infected
365 mice treated with PX478 every 48h continued to display delayed recovery as compared to the RSV
366 control mice (Fig. 1F). This was surprising as these RSV infected mice effectively cleared the virus
367 from the lung tissue and show no signs of increased inflammatory activity. One possible explanation
368 for the phenomenon could be a moderate appetite suppression induced by PX478 that is amplified
369 due to the stress of infection.

370 Treatment with PX478 in RSV infected mice resulted in initial antiviral activity regardless of
371 the PX478 dosing schedule. This was followed by prolonged viral replication at later time points of
372 infection when PX478 was given QD, but not QAD. Concurrently, these mice experienced a significant
373 reduction in the number of total cells present in the BAL, more strikingly in the number of lymphocytes.
374 HIF-1α is critical for the activation, migration, and cytotoxic functions of T-cells [29]. T-cells play an
375 important role in controlling RSV replication and clearance within the host [20-22]. During the early
376 stages of RSV disease, $CD4^+$ effector cells are known to aid in the recruitment and activation of other
377 immune cells that control RSV replication such as natural killer (NK) cells, $CD8^+$ cytotoxic T-cells,
378 and B-cells [30-32]. At later stages of disease, $CD8^+$ effector T-cells are responsible for directly
379 clearing RSV from the lung epithelium [33]. RSV/PXQAD mice had a significant reduction of total
380 leukocytes, total $CD4^+$ T-cells, and total $CD8^+$ T-cells at both timepoints assessed. Furthermore, during
381 peak of viral replication, the absolute and percentage of active and effector $CD4^+$ T-cells were
382 significantly reduced. Similarly, PXQAD treatment resulted in significantly reduced number of active
383 and effector $CD8^+$ T-cells present during peak viral clearance in the lungs of infected mice. Despite
384 the overall impact on the T-cell population, the RSV/PXQD and RSV/PXQAD treated mice displayed
385 antiviral activity at early and/or peak timepoints of RSV replication. Given the suppressed T-cell
386 activity, this antiviral effect is more likely attributed to impaired RSV replication rather than immune-
387 mediated activity. Aligning with our previous *in vitro* findings, the current study shows that HIF-1α
388 inhibition in RSV-infected mice influences the expression of genes that regulate critical metabolic
389 pathways, including glycolysis, an essential pathway for RSV replication in airway epithelial cells [15].
390 This likely contributes to the reduced RSV replication at early and peak timepoints in mice, rather than
391 immune-mediated activity.

392 Several studies have shown $CD8^+$ T-cells to be responsible for the clearance of RSV from the
393 lung tissue [33]. In our PXQD model, RSV replication is prolonged, indicating that the amount of virus

394 that can replicate is not being cleared from the lung tissue (Fig S1). $CD8^+$ T-cells were found to be
395 further suppressed in the RSV/PXQD mice when compared to the RSV/PXQAD mice (data not
396 shown). These results would suggest continuous treatment with PX478 to result in a threshold effect
397 of $CD8^+$ T-cell suppression, preventing efficient viral clearance. This is an important finding,
398 considering the use of HIF modulating therapeutics in the context of other diseases, such as cancer.

399 In contrast to HIF-1α, inhibition of HIF-2α by PT2385 was found to improve clinical disease,
400 with no difference in airway function. Like PX478, treatment with PT2385 demonstrated significant
401 antiviral activity at early and peak timepoints of RSV replication, with no impact on viral clearance.
402 Based on our previous characterizations in epithelial cells, where inhibition of HIF-2α did not affect
403 metabolic reprogramming and viral replication [15], the mechanisms underlying this activity could be
404 distinct from the ones responsible for impaired replication following HIF-1α inhibition.

405 RSV/PT2385 mice displayed a moderate increase in immune cell presence in the airway space.
406 This was characterized by an increased number of BAL macrophages and lymphocytes as well as lung
407 neutrophils and active $CD4^+$ and $CD8^+$ T-cells. Neutrophilic responses have been shown to contribute
408 to the control of viral replication in several models of respiratory virus infection, including RSV,
409 influenza, and SARS-CoV-2 [34-37], although other unidentified mechanism(s) are likely to play an
410 important role in the early antiviral activity observed with PT2385 administration. Recent studies found
411 that a loss of HIF-2α in regulatory T-cells (Treg) was associated with reduced suppressor functions,
412 leading to an increase in $CD4^+$ T-cell activity, without changes in Treg development [38, 39]. In
413 agreement with this finding, our results indicate an increase in $CD4^+$ and $CD8^+$ T-cell number,
414 including active/effector cells, with no significant alteration to Treg cell numbers (data not shown),
415 compared to the RSV/PBS control mice. As for other models of infection/inflammation, loss of HIF
416 protein activation in myeloid cells in a model of Leishmania infection also resulted in heightened $CD4^+$
417 Th1 immune response [40], and mice with T-cell intrinsic HIF-2α deletion showed exacerbated

418 intestinal inflammation, in a model of experimental colitis [41]. Since HIF-2α was shown to be
419 dispensable for RSV replication in epithelial cells, it is possible that this increase in immune cell
420 responses, both innate and adaptive, could play a major role in the observed antiviral effect seen in
421 RSV/PT2385 mice.

422 HIF-1α activation has been demonstrated to impact airway function in a variety of ways,
423 including the induction of bronchoconstriction [42]. HIF-1α achieves this by influencing the
424 contractility of airway smooth muscles through several mechanisms such as stimulating calcium
425 production, modulating ion channels, and triggering the release of mediators like leukotrienes [43-45].
426 In contrast, HIF-2α has been shown to be dispensable for the induction of changes to airway
427 hypersensitivity and bronchoconstriction [38]. Consistent with these findings, we observed notable
428 improvements in bronchoconstriction in RSV-infected mice treated with PX478 but not with PT2385.
429 In the PXQAD experiments, pathology scores for perivasculitis and peribronchiolitis were significantly
430 improved on days 4 and 7 p.i., as compared to the RSV control mice. This finding is consistent with
431 the reduced immune cell infiltration and antiviral activity at these timepoints. As HIF-1α has important
432 roles at the later stages of lung injury in promoting angiogenesis and tissue regeneration [46], it is
433 possible that inhibition of HIF-1α at the later stages of disease may hinder proper tissue repair, negating
434 the benefit observed in the initial phase of RSV lung disease. Mice treated with PT2385 during RSV
435 infection had no major alterations to any scored histopathology category until day 10 p.i., despite the
436 observed increase in BAL cellularity and increased T-cell recruitment to the lung, which could possibly
437 explain the lack of improvement in airway function of these mice. By the end of the acute phase,
438 RSV/PT2385 mice had a mild increase in perivasculitis, but significant improvements in all other
439 categories. This increase in perivasculitis could be due to the increase in the number of immune cells
440 observed within the BAL and lung tissue, but could also be related to changes in vascular function, as
441 HIF-2α plays an important role in maintaining the vascular integrity [47].

442

443 With the growing appreciation for the viral manipulation of the HIF pathway and the targeted
444 therapeutic potential, several studies have begun to investigate the contribution of HIF proteins to
445 diseases associated with other respiratory viruses. SARS-CoV-2 infection was found to induce
446 stabilization of HIF-1α in immune cells, via mitochondrial damage, facilitating viral replication and
447 cytokine production [48]. On the other hand, HIF activation via the prolyl hydroxylase inhibitor
448 Roxadustat reduced angiotensin-converting enzyme 2 (ACE2) expression and inhibited SARS-CoV-
449 2 entry and replication both in lung epithelial cells [49], as well as in a hamster model of infection
450 [50]. *In vitro*, IAV infection induces HIF stabilization via inhibition of the proteosome and decreased
451 expression of factor-inhibiting-HIF (FIH), with no changes in HIF-1α mRNA transcription or
452 hydroxylation [51], with pharmacological inhibition of HIF significantly reducing viral replication
453 [52]. In contrast, HIF-1α deficiency in lung epithelium was found to facilitate viral replication in a
454 mouse model of influenza A virus infection by promoting autophagy [53].

455 Collectively, our data demonstrate HIF-1α and HIF-2α to be important regulators of the
456 immune response to RSV infection. We also highlight HIF-1α as a critical component to the onset of
457 RSV-induced bronchoconstriction. Additionally, these data describe the novel and complex
458 contribution of the HIF-α subunits to RSV replication and clearance. Though we show antiviral
459 potential for both HIF-α inhibitors, the resulting impact to clinical disease and modulation of the
460 immune responses warrant great care be taken when considering HIF-α inhibitors for therapeutic use
461 against a viral respiratory infection. Furthermore, our data demonstrates that the continued inhibition
462 of HIF-1α can result in prolonged viral replication, highlighting the possible unwanted side effects
463 associated with the use of HIF modulating therapeutics in the context of other diseases, such as cancer.

464 Future investigations will focus on further understanding the mechanistic contribution of the different

465 HIF alpha subunits to the immune response and tissue repair processes during RSV infection.

466 **6 Conflict of Interest**

467 The authors declare that the research was conducted in the absence of any commercial or
468 financial relationships that could be construed as a potential conflict of interest.

469 **7 Author Contributions**

470 Performed experiments, D.R.M., Y.Q., T.I., M.W., A.H.M., and T.L; performed histopathology
471 analysis, Y.L.J.H; contributed to data analysis and drafting of the manuscript, D.R.M. and A.H.M.;
472 contributed to the conception of the manuscript, literature review, and final manuscript editing,
473 D.R.M., A.C. and R.P.G. All authors have read and agreed to the published version of the
474 manuscript.

475 **8 Funding**

476 DRM was supported by the McLaughlin Endowment Predoctoral Fellowship and the NIH
477 Clinical and Translational Science Award NRSA (TL1) Training Core TL1TR001440. This research
478 was additionally funded by an Institute for Human Infections and Immunity (IHII) Pilot Grant and by
479 NIH grants AI62885 and AI175955.

480 **9 Acknowledgments**

481 We would like to thank Vineet Menachery, Yuejin Liang, Casey Wright, and Xiaoyi Yuan for
482 their thoughtful discussion. We would also like to thank the Texas A&M University Veterinary
483 Medicine and Biomedical Sciences Research Histology Core Facility for their assistance with the tissue
484 processing. Biorender.com was used to produce the experimental design summaries.

485 **10 Supplementary Material**

486

11 Figures

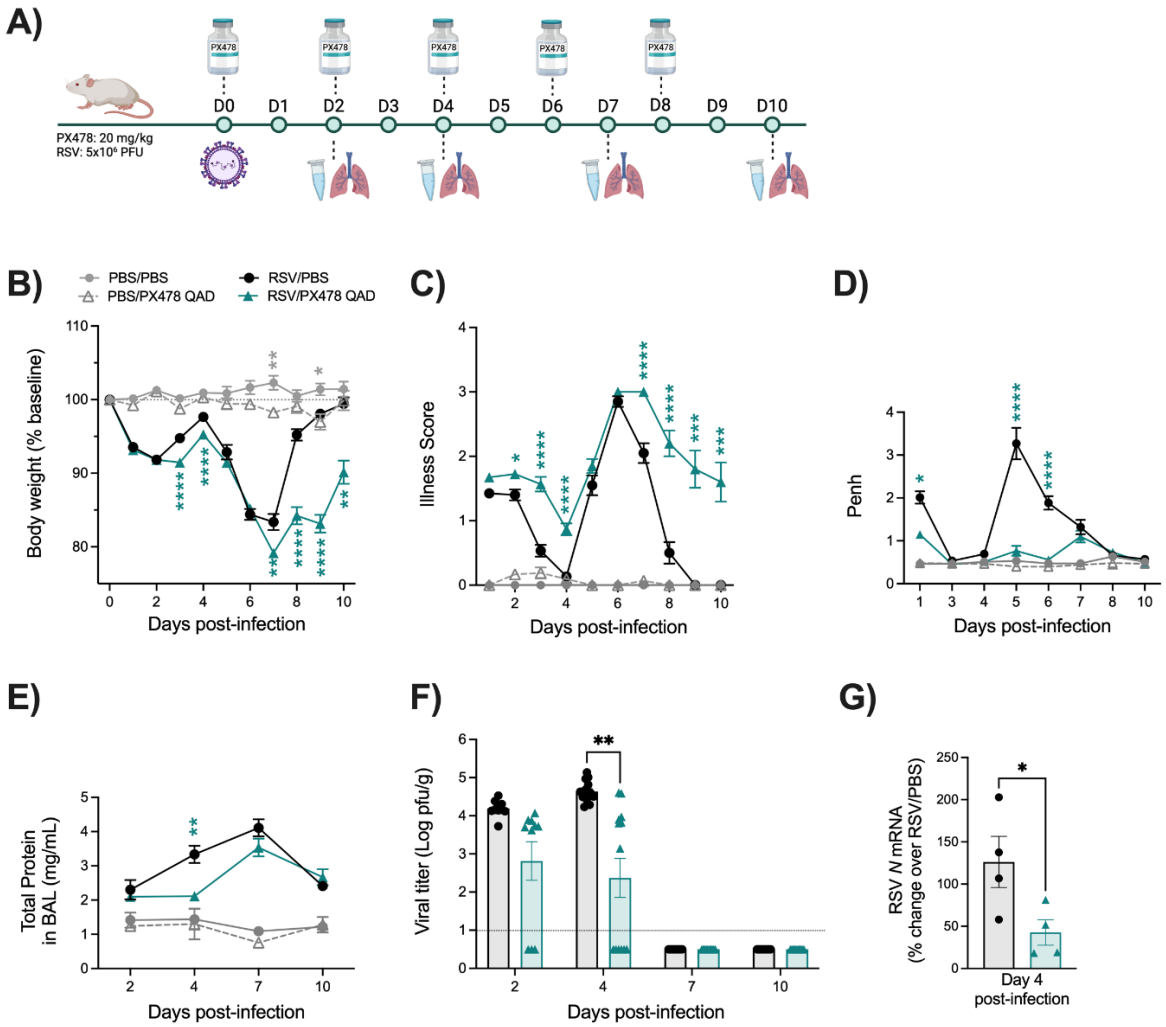

Figure 1. *Assessment of clinical disease, airway function, and viral replication following HIF-1α inhibition during RSV infection.* The experimental design for mice treated with PX478 QAD is described in (A). Following treatment, all mice were monitored daily for changes in (B) body weight and (C) illness score. (D) Bronchoconstriction, represented by baseline Penh, was measured by plethysmography. At days 2, 4, 7, and 10 p.i., (E) total protein was measured in the BAL fluid and the lung was collected for assessment of (F) viral replication by plaque assay. At day 4 p.i, (G) RSV *N* mRNA levels were measured by RT-qPCR. For clinical disease, data are pooled from four independent experiments (PBS/PBS n = 6-8, PBS/PX n = 6-18, RSV/PBS n = 10-30, RSV/PX n = 9-30 mice/group). For bronchoconstriction, data are pooled from three independent experiments (PBS/PBS and PBS/PX n = 6-12, RSV/PBS and RSV/PX n = 6-30 mice/group). For total protein, data are pooled from two independent experiments (PBS/PBS and PBS/PX n = 4-6, RSV/PBS and RSV/PX n = 8-10 mice/group). For viral replication by plaque assay, data are pooled from two independent experiments (n = 10-14 mice/group). For RT-qPCR data are from one independent experiment (n = 4 mice/group). Data are expressed as mean ± SEM. Significant results were determined by two-way mixed ANOVA (B-F) and unpaired t test (G) (* $p \leq 0.05$, ** $p \leq 0.01$, *** $p \leq 0.001$, **** $p \leq 0.0001$).

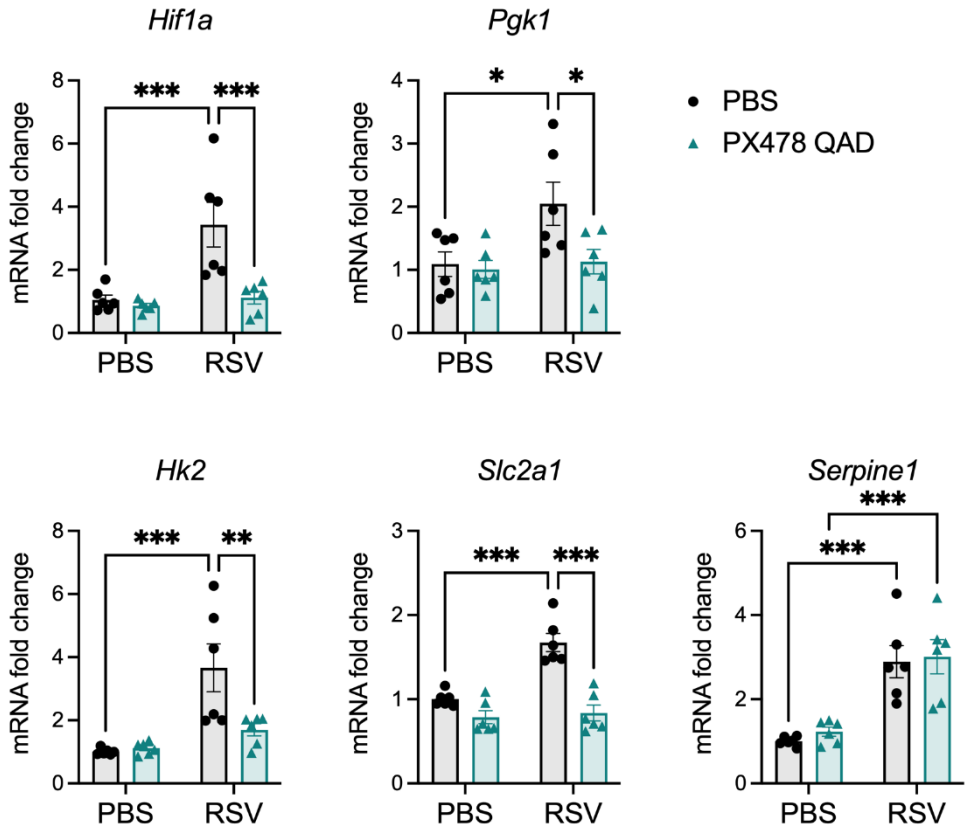

503

504 **Figure 2.** *Effect of PX478 on Hif1a and HIF-1α and -2α target genes in the lungs of mice during RSV*
505 *infection.* Mice were euthanized at day 2 p.i. and RNA was extracted from the lung tissue. *Hif1a*, the
506 HIF-1α targets *Pgk1*, *Hk2*, and *Slc2a1* (GLUT1), and the HIF-2α target *Serpine1* (PAI-1) gene
507 expression was measured by RT-qPCR (n = 6 mice/group). Data are expressed as mean ± SEM.
508 Significant results were determined by two-way ANOVA followed by Bonferroni's multiple
509 comparisons test (* $p \leq 0.05$, ** $p \leq 0.01$, *** $p \leq 0.001$).

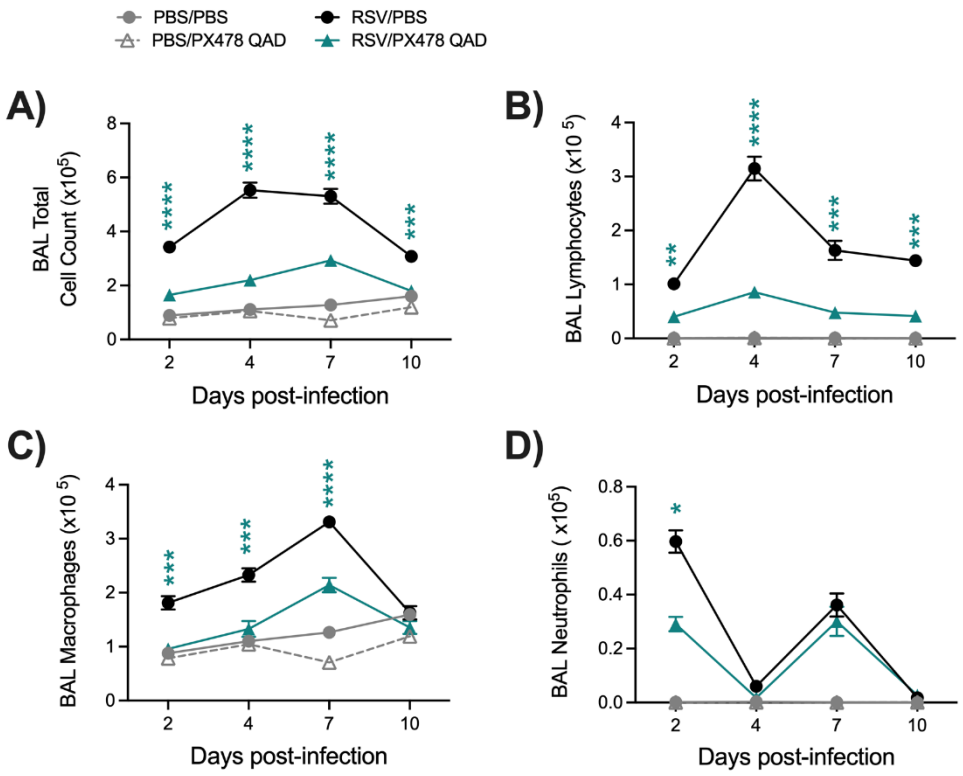

510

511 **Figure 3.** *Differential cell count of the BAL fluid following HIF-1α inhibition during RSV infection.*
512 At days 2, 4, 7, or 10 p.i., BAL fluid was collected from mice that had been treated or not with PX478
513 QAD. This BAL was used to obtain (A) total cell counts, as well as differential cell counts consisting
514 of (B) lymphocytes, (C) macrophages, and (D) neutrophils. Data are pooled from two independent
515 experiments (PBS/PBS and PBS/PX478 n = 4-6, RSV/PBS and RSV/PX478 n = 10 mice/group). Data
516 are expressed as mean ± SEM. Significant results were determined by two-way mixed ANOVA (* $p \leq$
517 0.05, ** $p \leq 0.01$, *** $p \leq 0.001$, **** $p \leq 0.0001$).

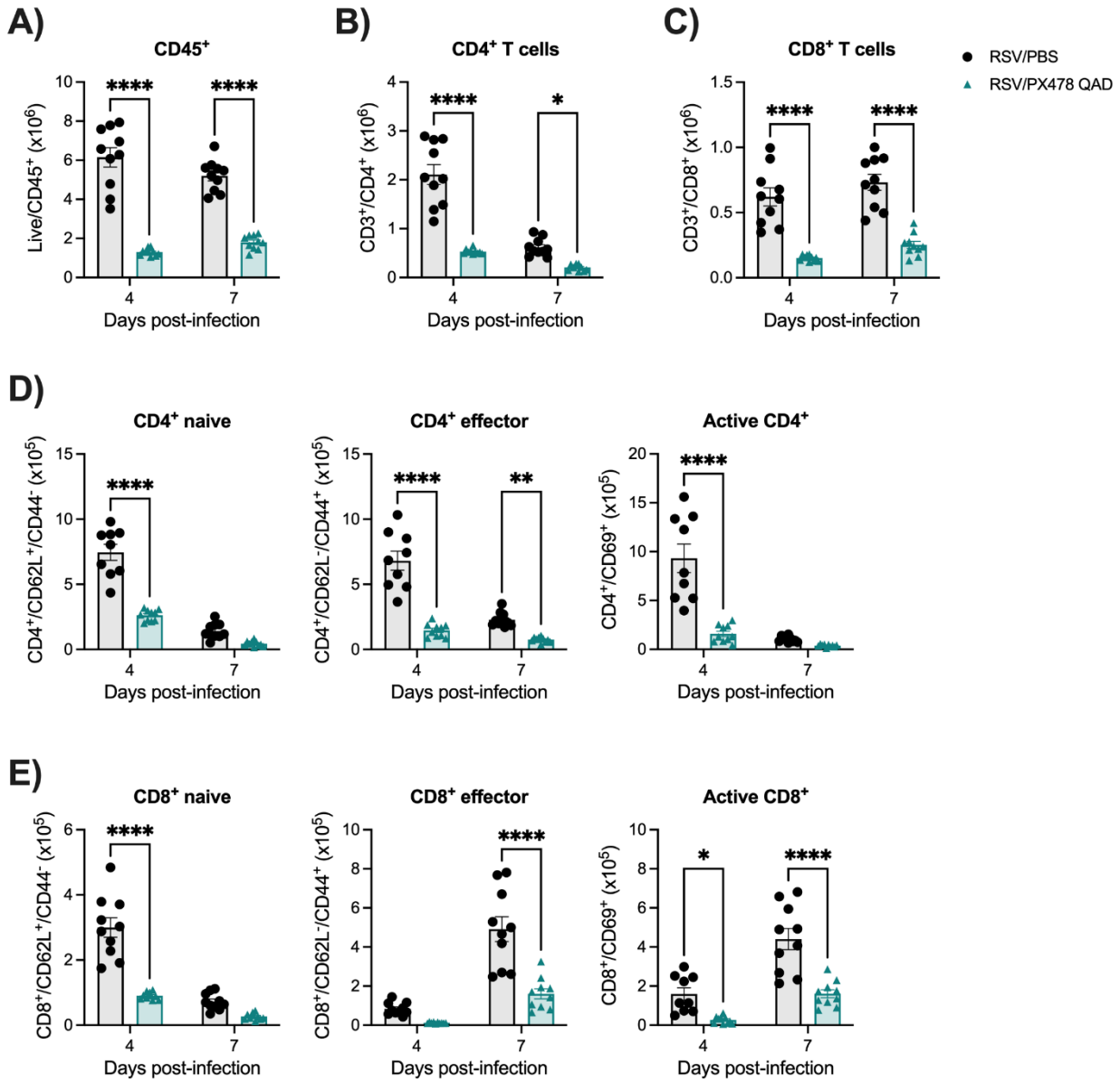

518

519 **<u>Figure 4.</u>** *Assessment of CD4⁺ and CD8⁺ T cells following HIF-1α inhibition during RSV infection.*
520 Whole lung tissue was collected at peak RSV replication and a timepoint of viral clearance, days 4 and
521 7 p.i., respectively. Single cell suspension was prepared, stained with live/dead cell dye and
522 fluorochrome-conjugated antibodies, and acquired by flow cytometry. Data were analyzed following
523 the gating strategy in Figure S2. Quantification of absolute cell counts of (A) Live $CD45^+$, (B) $CD4^+$
524 T cells, (C) $CD8^+$ T cells, (D) $CD4^+$ naive, effector, and active, and (E) $CD8^+$ naive, effector, and active
525 cells are shown. Data are pooled from two independent experiments (n = 9-10 mice/group). Data are
526 expressed as mean ± SEM. Significant results were determined by two-way mixed ANOVA (* $p \leq$
527 0.05, ** $p \leq 0.01$, *** $p \leq 0.001$, **** $p \leq 0.0001$).

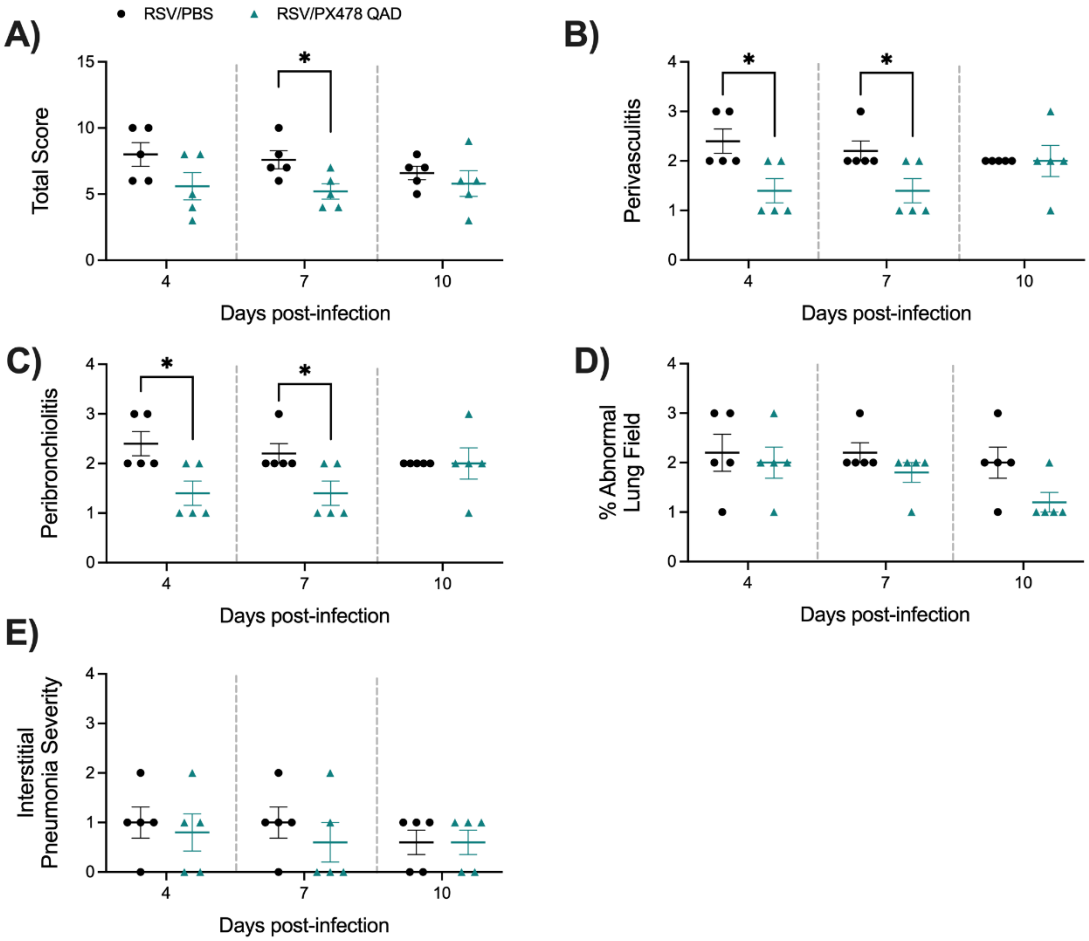

528

529 **Figure 5.** *Histopathological scoring of lung tissue following HIF-1α inhibition during RSV infection.*
530 At days 4, 7, and 10 p.i., the left lung was collected from RSV infected mice that had received PBS
531 or PX478 QAD and subjected to FFPE. Cuts of lung tissue were stained with H&E and observed
532 under a microscope at 10X magnification. The (A) total score was calculated, consisting of scores for
533 (B) perivasculitis, (C) peribronchiolitis, (D) percent abnormal lung field, and (E) interstitial
534 pneumonia. Data are representative of one independent experiment (n = 5 mice/group). Data are
535 expressed as mean ± SEM. Significant results were determined by an unpaired student's t-test (* $p \leq$
536 0.05).

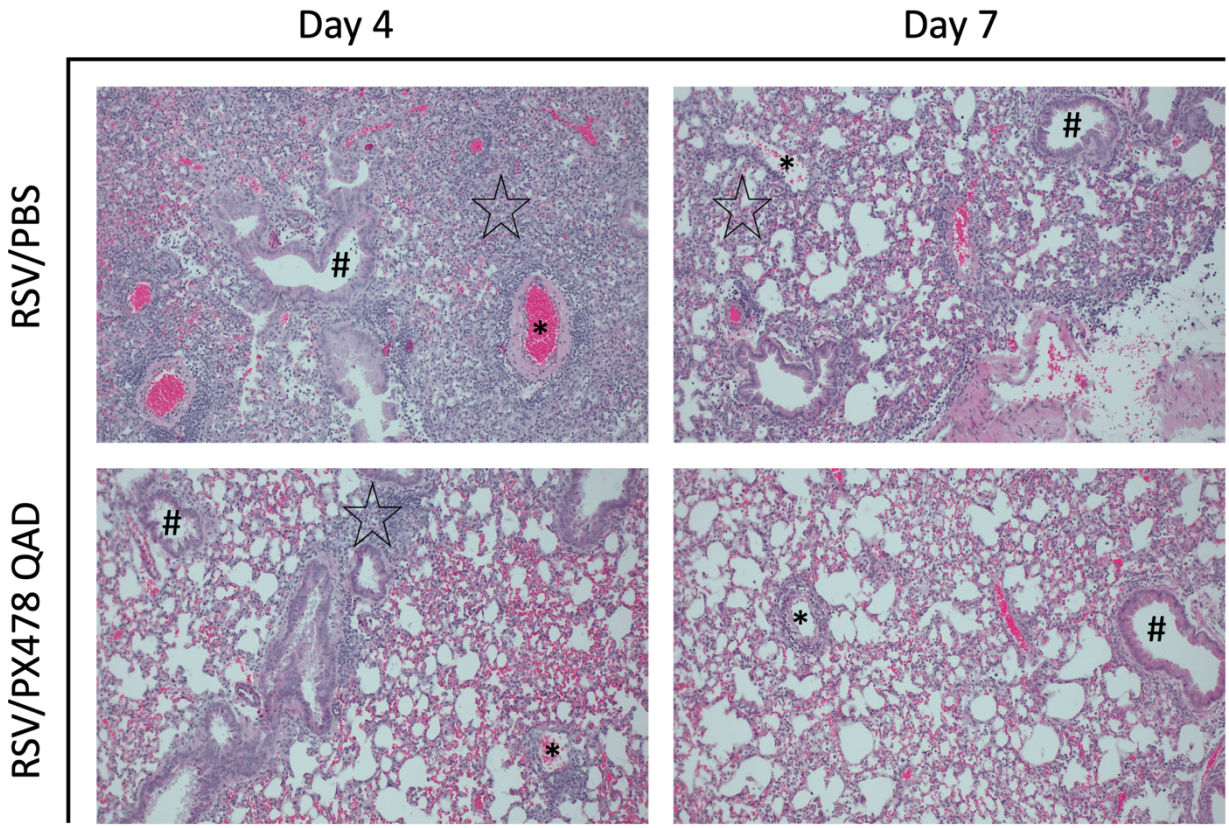

537

538 **Figure 6.** *Histopathological imaging of lung tissue following HIF-1α inhibition during RSV infection.*

539 At days 4 and 7 p.i., the left lung was collected from mice that had received PBS or PX478 every 48 h

540 and subjected to FFPE. Cuts of lung tissue were stained with H&E and observed under a microscope

541 at 10X magnification. Perivasculitis is indicated by an asterisk. Peribronchiolitis is indicated by the

542 hash sign. Interstitial pneumonia is indicated by the black star. No interstitial pneumonia present in

543 RSV/PX478 QAD on day 7. Representative images are shown here (n = 5 mice/group).

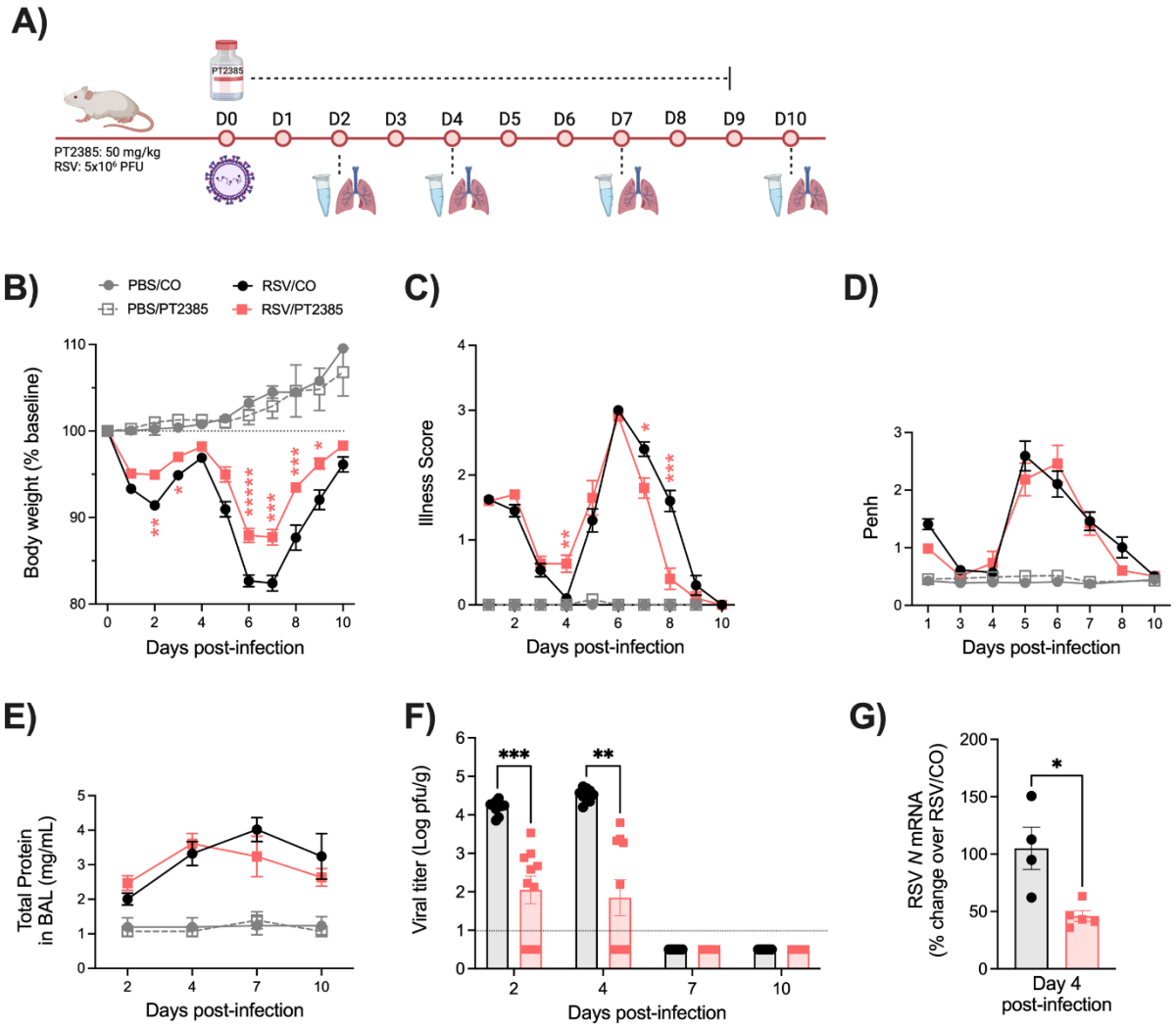

Figure 7. *Assessment of clinical disease, airway function, and viral replication following HIF-2α inhibition during RSV infection.* The experimental design for mice treated with PT2385 is described in (A). Following treatment, all mice were monitored daily for changes in (B) body weight and (C) illness score. (D) Bronchoconstriction, represented by baseline Penh, was measured by plethysmography. At days 2, 4, 7, and 10 p.i., (E) total protein was measured in the BAL fluid and the right lung was collected for assessment of (F) viral replication by plaque assay. At day 4 p.i, (G) RSV *N* mRNA levels were measured by RT-qPCR. For clinical disease, data are pooled from four independent experiments (PBS/CO n = 6-12, PBS/PT n = 6-18, RSV/CO n = 6-24, RSV/PT n = 6-24 mice/group). For bronchoconstriction, data are pooled from three independent experiments (PBS/CO and PBS/PT n = 6-12, RSV/CO and RSV/PT n = 6-24 mice/group). For total protein, data are pooled from two independent experiments (PBS/CO and PBS/PT n = 4-5, RSV/CO and RSV/PT n = 5-10 mice/group. For viral replication by plaque assay, data are pooled from two independent experiments (n = 9-10 mice/group). For RT-qPCR, data are from one independent experiment (n = 4-5 mice/group). Data are expressed as mean ± SEM. Significant results were determined by two-way mixed ANOVA (B-F) and unpaired t test (G) (* $p \leq 0.05$, ** $p \leq 0.01$, *** $p \leq 0.001$, **** $p \leq 0.0001$).

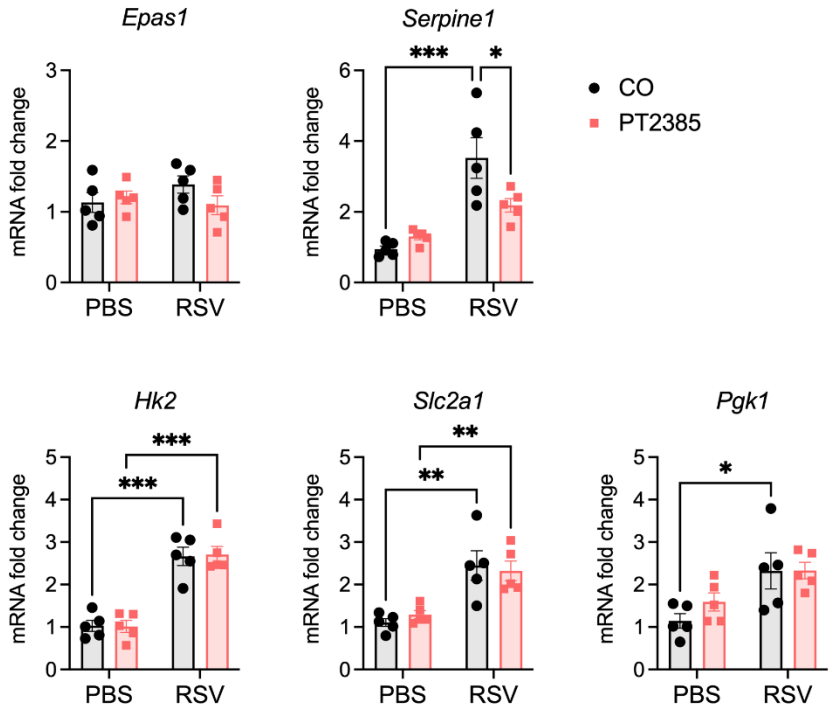

Figure 8. *Effect of PT2385 on Epas1 (HIF-2α) and HIF-1α and -2α target genes in lungs of mice during RSV infection.* A group of mice were euthanized at day 2 p.i., lungs were harvested, and total lung RNA was extracted. *Epas1* (HIF-2α), the HIF-2α target *Serpine1* (PAI-1), and the HIF-1α targets *Pgk1, Slc2a1* (GLUT1) and *Hk2* gene expression was measured by RT-qPCR (n = 5 mice/group). Data are expressed as mean ± SEM. Significant results were determined by two-way ANOVA followed by Bonferroni's multiple comparisons test (* $p \leq 0.05$, ** $p \leq 0.01$, *** $p \leq 0.001$).

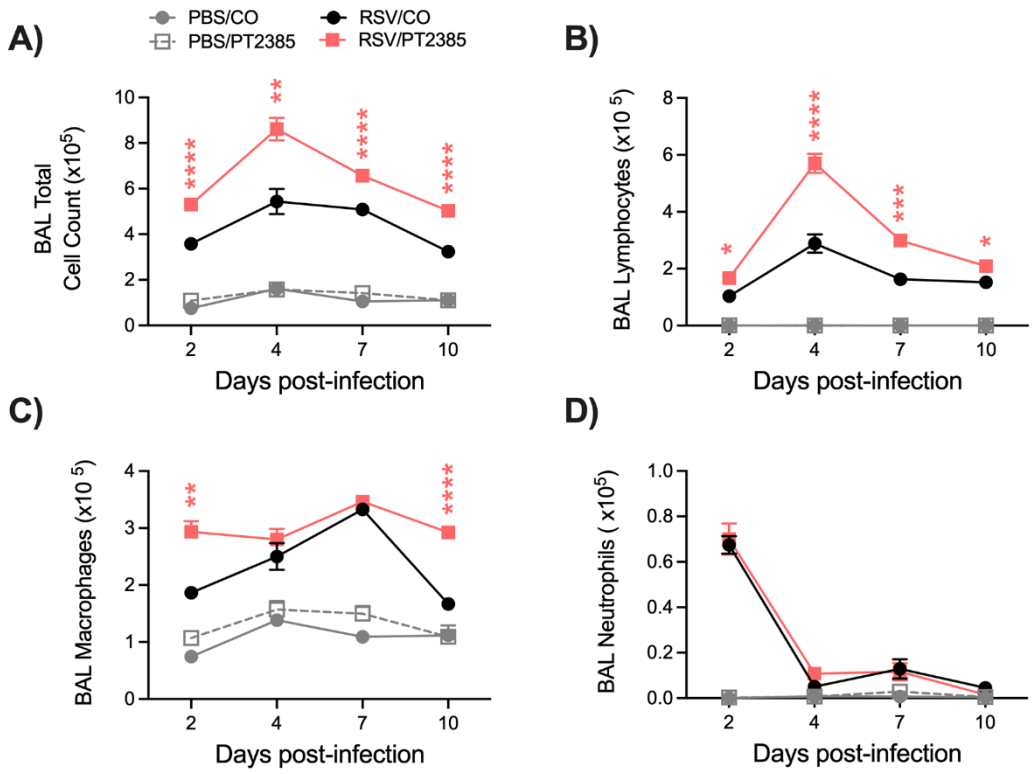

567

568 **Figure 9.** *Differential cell count of the BAL fluid following HIF-2α inhibition during RSV infection.*
569 At days 2, 4, 7, and 10 p.i., BAL fluid was collected and used to obtain (A) total cell counts, as well as
570 differential cell counts consisting of (B) lymphocytes, (C) macrophages, and (D) neutrophils. Data are
571 pooled from two independent experiments (PBS/CO and PBS/PT n = 4-6, RSV/CO and RSV/PT n =
572 10-15 mice/group). Data are expressed as mean ± SEM. Significant results were determined by mixed-
573 effects analysis (* $p \leq 0.05$, ** $p \leq 0.01$, *** $p \leq 0.001$, **** $p \leq 0.0001$).

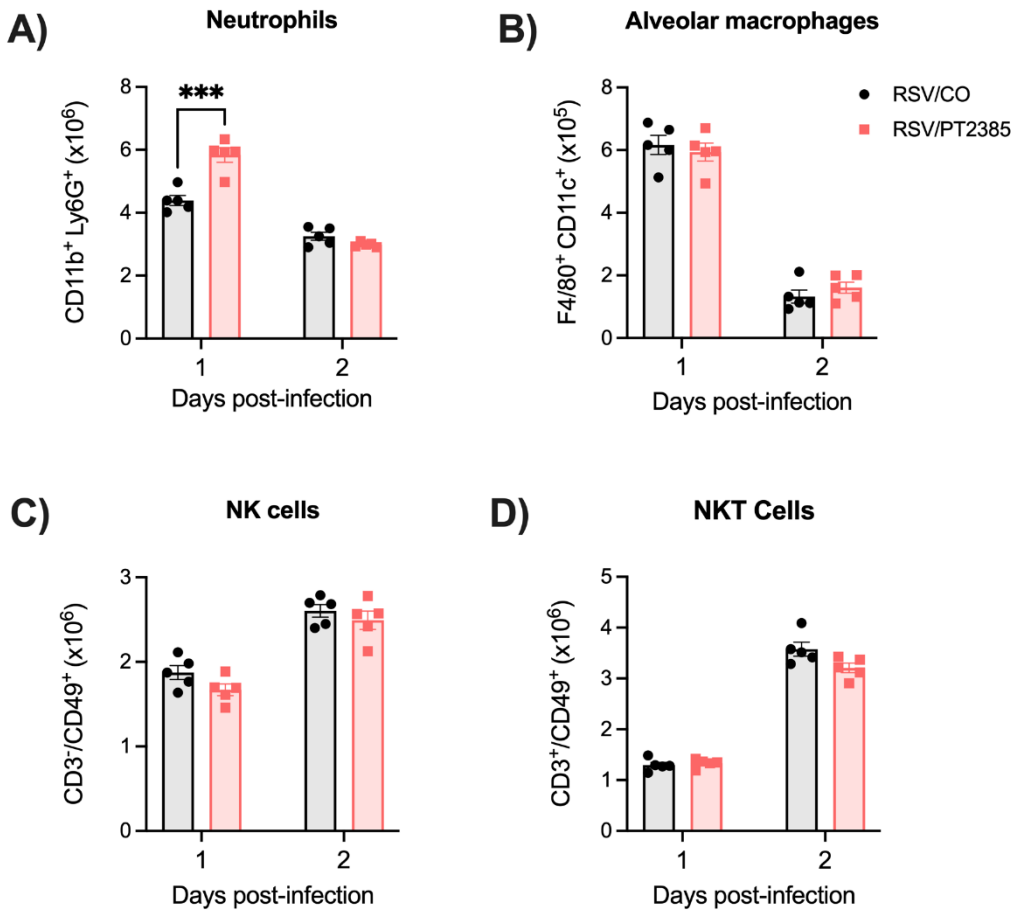

Figure 10. *Assessment of neutrophils, alveolar macrophages, natural killer, and NKT cells following HIF-2α inhibition during RSV infection.* Mice were euthanized at days 1 and 2 p.i., and whole lung tissue was collected. Single cell suspension was prepared, stained with live/dead cell dye and fluorochrome-conjugated antibodies, and acquired by flow cytometry. Data were analyzed following the gating strategy in Figure S3. Shown here are absolute cell counts for (A) neutrophils, (B) alveolar macrophages, (C) NK cells, and (D) NKT cells. Data are expressed as mean ± SEM (n = 5 mice/group). Significant results were determined by two-way ANOVA (*** $p \leq 0.001$).

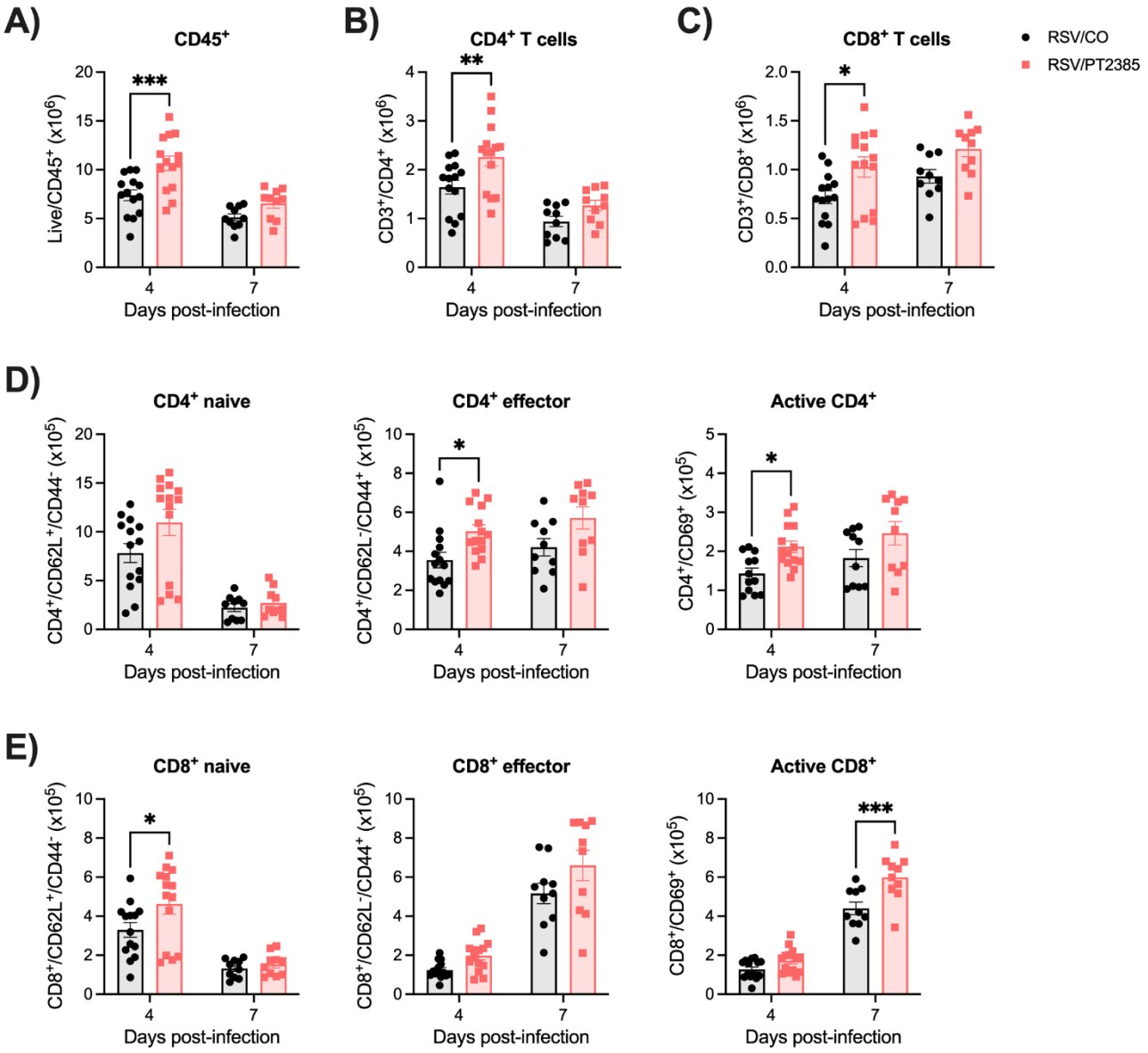

Figure 11. *Assessment of CD4⁺ and CD8⁺ T-cells following HIF-2α inhibition during RSV infection.* Whole lung tissue was collected at peak RSV replication and a timepoint of viral clearance, days 4 and 7 p.i., respectively. Single cell suspension was prepared, stained with live/dead cell dye and fluorochrome-conjugated antibodies, and acquired by flow cytometry. Data were analyzed following the gating strategy in Figure S2. Quantification of absolute cell counts of (A) Live $CD45^+$, (B) $CD4^+$ T cells, (C) $CD8^+$ T cells, (D) $CD4^+$ naive, effector, and active, and (E) $CD8^+$ naive, effector, and active cells are shown. Data are pooled from two to three independent experiments (n = 10-14 mice/group). Data are expressed as mean ± SEM. Significant results were determined by a two-way mixed ANOVA (* $p \leq 0.05$, ** $p \leq 0.01$, *** $p \leq 0.001$).

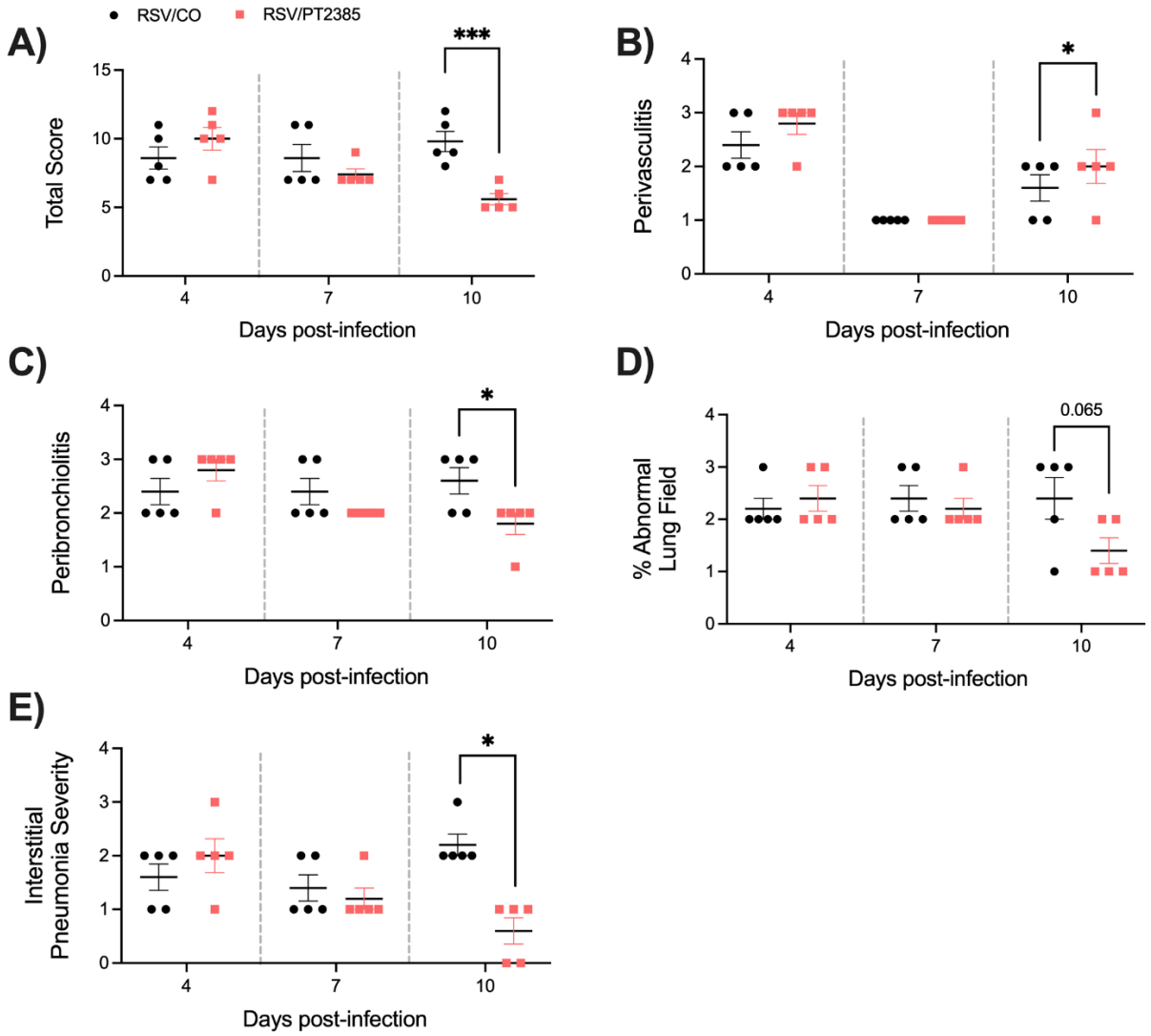

592

593 **Figure 12.** *Histopathological scoring of lung tissue following HIF-2α inhibition during RSV infection.*
594 At days 4, 7, and 10 p.i., the left lung was collected from RSV infected mice that had received CO or
595 PT2385 and subjected to FFPE. Cuts of lung tissue were stained with H&E and observed under a
596 microscope at 10X magnification. The (A) total score was calculated, consisting of scores for (B)
597 perivasculitis, (C) peribronchiolitis, (D) percent abnormal lung field, and (E) interstitial pneumonia.
598 Data are representative of one independent experiment (n = 5 mice/group). Data are expressed as mean
599 ± SEM. Significant results were determined by an unpaired student's t-test (* $p \leq 0.05$, *** $p \leq 0.001$).

600

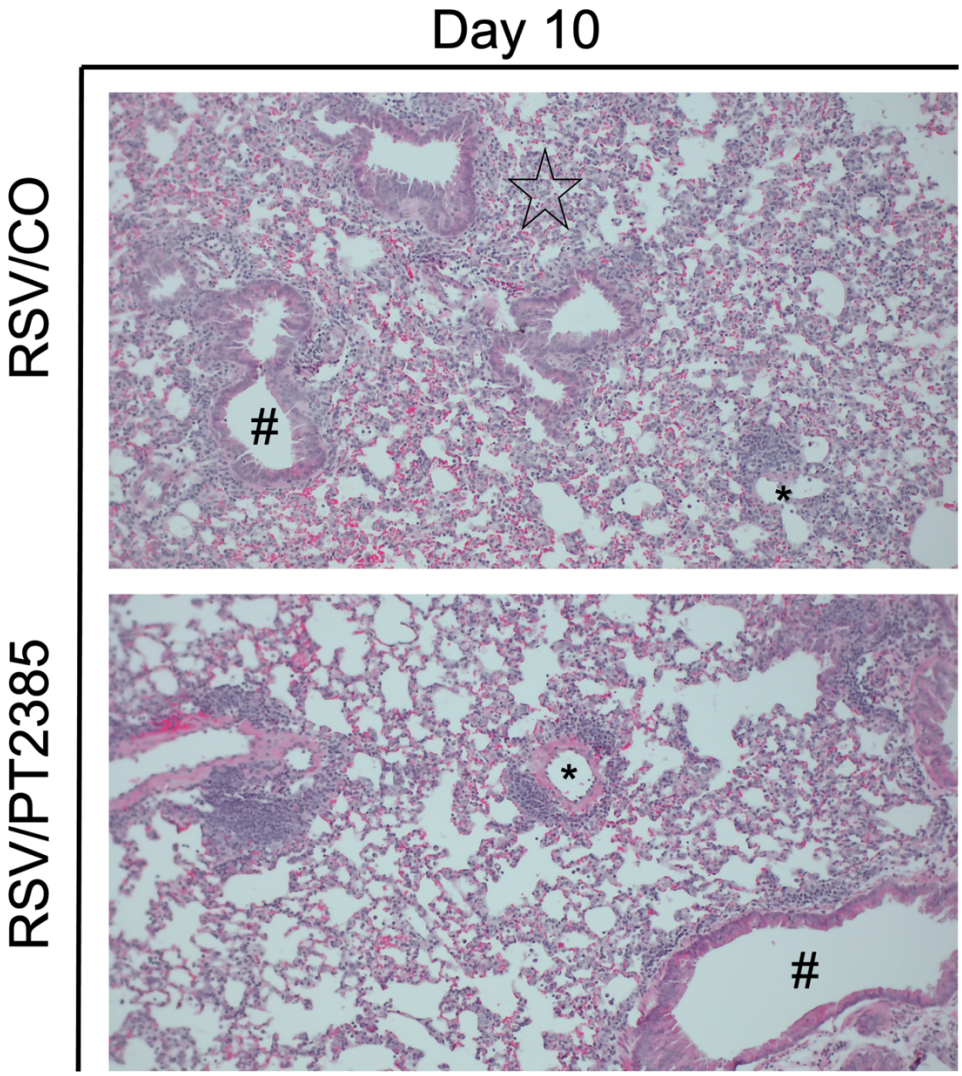

601

602 **Figure 13.** *Histopathological images of lung tissue following HIF-2a inhibition during RSV infection.*
603 At day 10 p.i., the left lung was collected from mice that had received PBS or PT2385 and subjected
604 to FFPE. Cuts of lung tissue were stained with H&E and observed under a microscope at 10X
605 magnification. Perivasculitis is indicated by an asterisk. Peribronchiolitis is indicated by the hash
606 symbol. Interstitial pneumonia is indicated by the black star. No interstitial pneumonia present in
607 RSV/PT2385. Representative images are shown here (n = 5 mice/group).

608

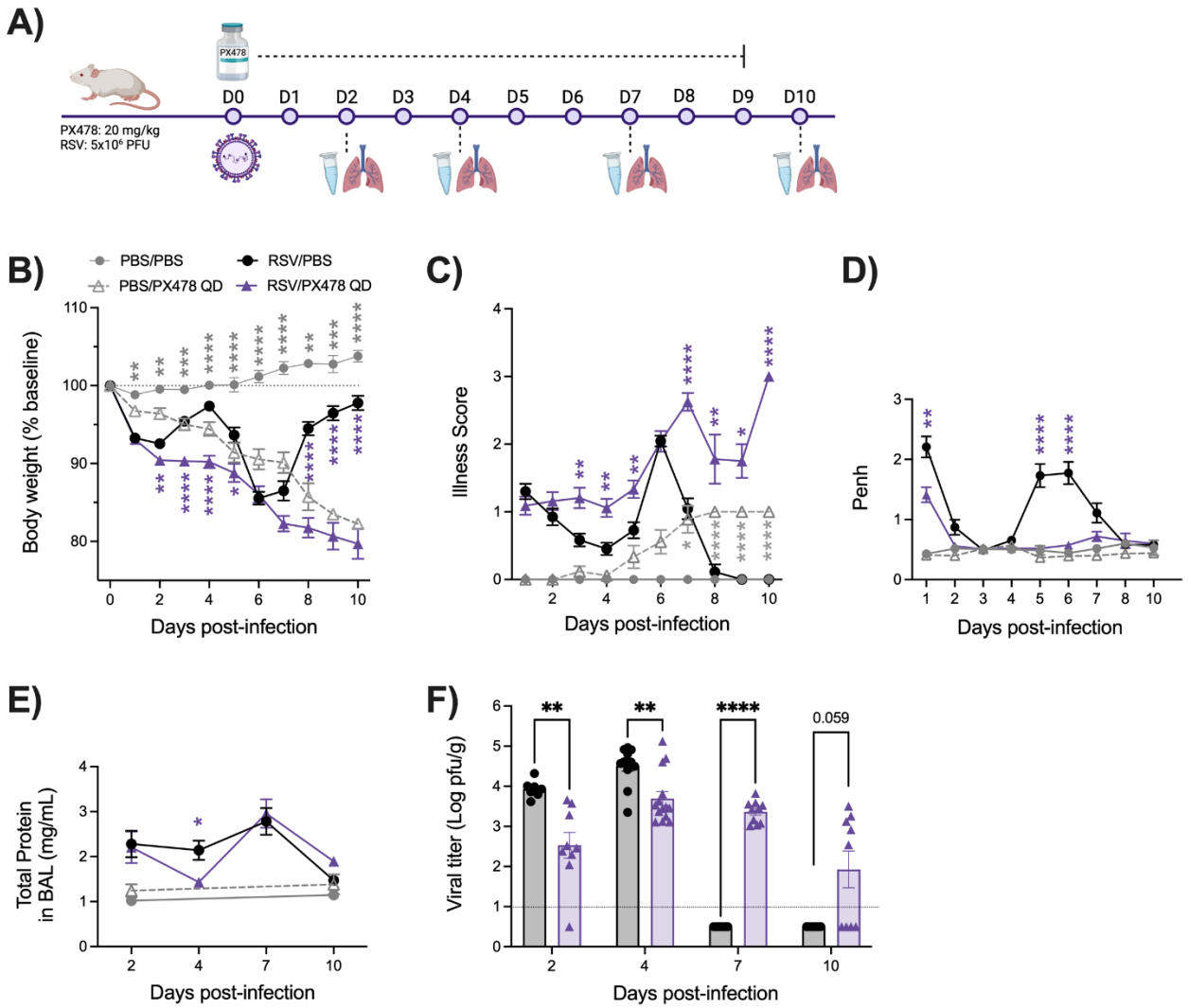

Figure S1. *Assessment of clinical disease, airway function, and viral replication following HIF-1a inhibition during RSV infection.* The experimental design for mice treated with PX478 QD is described in (A). Following treatment, all mice were monitored daily for changes in (B) body weight and (C) illness score. (D) Bronchoconstriction, represented by baseline Penh, was measured by plethysmography. At days 2, 4, 7, and 10 p.i., (E) total protein was measured in the bronchoalveolar lavage (BAL) fluid and the right lung was collected for assessment of (F) viral replication by plaque assay. For clinical disease, data are pooled from four independent experiments (PBS/PBS n = 6, PBS/PX n = 6-18, RSV/PBS and RSV/PX n = 6-24 mice/group). For bronchoconstriction, data are pooled from three independent experiments (PBS/PBS and PBS/PX n = 6, RSV/PBS and RSV/PX n = 6-24 mice/group). For total protein, data are pooled from two independent experiments (PBS/PBS and PBS/PX n = 4, RSV/PBS and RSV/PX n = 8-10 mice/group). For viral replication, data are pooled from two independent experiments (RSV/PBS n = 7-12, RSV/PX n = 9-14 mice/group). Data are expressed as mean ± SEM. Significant results were determined by two-way mixed ANOVA (* $p \leq 0.05$, ** $p \leq 0.01$, *** $p \leq 0.001$, **** $p \leq 0.0001$).

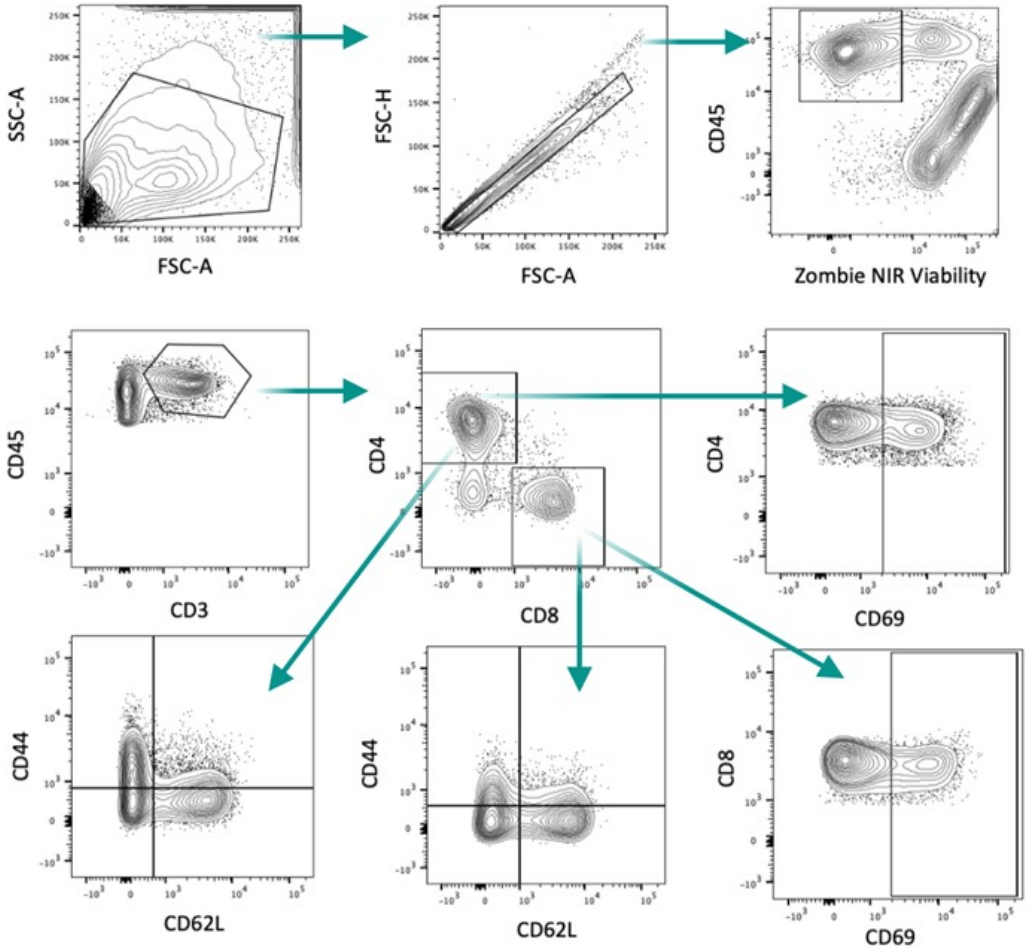

624

625 **Figure S2.** *Schematic for analysis of CD4⁺ and CD8⁺ T-cells by flow cytometry.* At days 4 and 7 p.i.,
626 whole lung tissue was collected from the respective groups. Single cell suspension was prepared,
627 stained with live/dead cell dye and fluorochrome-conjugated antibodies, followed by flow cytometric
628 analysis. T cells were gated on $CD45^+CD3^+$ first, then further gated on $CD4^+$ and $CD8^+$
629 subpopulations. Naïve and effector T cells were gated on $CD44^-CD62L^+$ and $CD44^+CD62L^-$,
630 respectively. CD69 was used as an early activation marker of T cells.

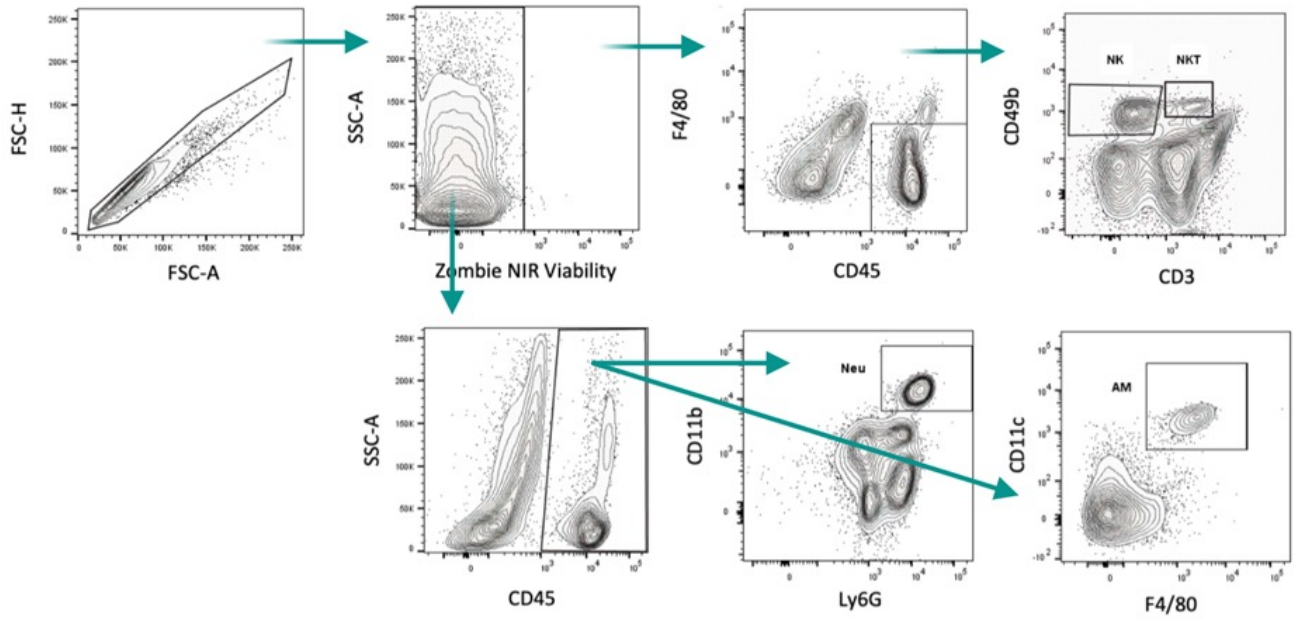

631

632 **Figure S3.** *Schematic for analysis of neutrophils, alveolar macrophages (AM), natural killer (NK),*
633 *and NKT cells by flow cytometry.* At days 1 and 2 p.i., whole lung tissue was collected from the
634 respective groups. Single cell suspension was prepared, stained with live/dead cell dye and
635 fluorochrome-conjugated antibodies, followed by flow cytometric analysis. After gating for
636 $Live^{+}/Dead^{-}$ followed by $F4/80^{-}CD45^{+}$ leukocytes, NK cells were gated on $CD3^{-}CD49^{+}$, and NKT
637 cells were gated on $CD3^{+}CD49^{+}$. After gating for $Live^{+}/Dead^{-}$ followed by $CD45^{+}$ leukocytes,
638 neutrophils were gated on $CD11b^{+}Ly6G^{+}$ and AMs were gated on $CD11c^{+}F4/80^{+}$.

639 **Table S1.** Percentages of $CD4^+$ and $CD8^+$ T cells subpopulations following HIF-1α inhibition at days
640 4 and 7 post RSV infection. Data from two independent experiments (n = 9-10 mice/group).

	RSV/PBS						RSV/PX478 QAD					
	Percentage from $CD4^+$			Percentage from $CD8^+$			Percentage from $CD4^+$			Percentage from $CD8^+$		
	Active	Eff	Naive	Active	Eff	Naive	Active	Eff	Naive	Active	Eff	Naive
D4	47.3	34.9	38.1	30.4	14.1	49.2	29.4	27.3	49.5	17.1	8.1	59.9
D7	16.8	37.7	22.5	58.8	65.2	10.0	18.7	37.1	20.9	62.9	61.0	10.6

641

642

643 **Table S2.** Percentages of $CD4^+$ and $CD8^+$ T cells subpopulations following HIF-2α inhibition at days
644 4 and 7 post RSV infection. Data from two to three independent experiments (n = 10-14 mice/group).

	RSV/CO						RSV/PT2385					
	Percentage from $CD4^+$			Percentage from $CD8^+$			Percentage from $CD4^+$			Percentage from $CD8^+$		
	Active	Eff	Naive	Active	Eff	Naive	Active	Eff	Naive	Active	Eff	Naive
D4	11.0	23.1	45.8	17.8	17.8	45.1	10.4	24.4	46.0	17.7	19.4	43.9
D7	19.3	45.6	22.3	47.6	54.4	14.0	19.0	44.8	20.5	49.7	53.4	12.3

645

646 **12 References**

647 1. Shi, T., et al., *Global, regional, and national disease burden estimates of acute lower*
648 *respiratory infections due to respiratory syncytial virus in young children in 2015: a*
649 *systematic review and modelling study.* The Lancet, 2017. **390**(10098): p. 946-958.

650 2. Kampmann, B., et al., *Bivalent Prefusion F Vaccine in Pregnancy to Prevent RSV Illness in*
651 *Infants.* New England Journal of Medicine, 2023. **388**(16): p. 1451-1464.

652 3. Papi, A., et al., *Respiratory Syncytial Virus Prefusion F Protein Vaccine in Older Adults.*
653 New England Journal of Medicine, 2023. **388**(7): p. 595-608.

654 4. Muller, W.J., et al., *Nirsevimab for Prevention of RSV in Term and Late-Preterm Infants.*
655 New England Journal of Medicine, 2023. **388**(16): p. 1533-1534.

656 5. Thaker, S.K., J. Ch'ng, and H.R. Christofk, *Viral hijacking of cellular metabolism.* BMC
657 Biology, 2019. **17**(1): p. 59.

658 6. Reyes, A., et al., *Contribution of hypoxia inducible factor-1 during viral infections.*
659 Virulence, 2020. **11**(1): p. 1482-1500.

660 7. Huang, R., et al., *Hypoxia and viral infectious diseases.* JCI Insight, 2021. **6**(7).

661 8. Semenza, G.L., *Pharmacologic Targeting of Hypoxia-Inducible Factors.* Annual Review of
662 Pharmacology and Toxicology, 2019. **59**(1): p. 379-403.

663 9. Reyes, A., et al., *Impact of Hypoxia over Human Viral Infections and Key Cellular Processes.*
664 Int J Mol Sci, 2021. **22**(15).

665 10. Brahimi-Horn, M.C. and J. Pouysségur, *HIF at a glance.* Journal of Cell Science, 2009.
666 **122**(8): p. 1055-1057.

667 11. Infantino, V., et al., *Cancer Cell Metabolism in Hypoxia: Role of HIF-1 as Key Regulator and*
668 *Therapeutic Target.* International Journal of Molecular Sciences, 2021. **22**(11): p. 5703.

669 12. Koh, M.Y. and G. Powis, *Passing the baton: the HIF switch.* Trends Biochem Sci, 2012.
670 **37**(9): p. 364-72.

671 13. Zhang, P., et al., *Hypoxia-Inducible Factor 3 Is an Oxygen-Dependent Transcription*
672 *Activator and Regulates a Distinct Transcriptional Response to Hypoxia.* Cell Reports, 2014.
673 **6**(6): p. 1110-1121.

674 14. Downes, N.L., et al., *Differential but Complementary HIF1alpha and HIF2alpha*
675 *Transcriptional Regulation.* Mol Ther, 2018. **26**(7): p. 1735-1745.

676 15. Morris, D.R., et al., *HIF-1alpha Modulates Core Metabolism and Virus Replication in*
677 *Primary Airway Epithelial Cells Infected with Respiratory Syncytial Virus.* Viruses, 2020.
678 **12**(10).

679 16. Ueba, O., *Respiratory syncytial virus. I. Concentration and purification of the infectious*
680 *virus.* Acta Med Okayama, 1978. **32**(4): p. 265-72.

681 17. Morris, D.R., et al., *Selective Blockade of TNFR1 Improves Clinical Disease and*
682 *Bronchoconstriction in Experimental RSV Infection.* Viruses, 2020. **12**(10).

683 18. Morris, D., et al., *Antiviral and Immunomodulatory Activity of Silver Nanoparticles in*
684 *Experimental RSV Infection.* Viruses, 2019. **11**(8).

685 19. Qu, Y., et al., *SARS-CoV-2 Inhibits NRF2-Mediated Antioxidant Responses in Airway*
686 *Epithelial Cells and in the Lung of a Murine Model of Infection.* Microbiol Spectr, 2023.
687 **11**(3): p. e0037823.

688 20. Russell, C.D., et al., *The Human Immune Response to Respiratory Syncytial Virus Infection.*
689 2017. **30**(2): p. 481-502.

690 21. De, C., et al., *Human T cells efficiently control RSV infection.* JCI Insight, 2023. **8**(11).

691 22. McGinley, J., et al., *A Systematic Review and Meta-analysis of Animal Studies Investigating*
692 *the Relationship Between Serum Antibody, T Lymphocytes, and Respiratory Syncytial Virus*
693 *Disease.* The Journal of Infectious Diseases, 2021. **226**(Supplement_1): p. S117-S129.

694 23. Morris, D.R., et al., *HIF-1α Modulates Core Metabolism and Virus Replication in Primary*
695 *Airway Epithelial Cells Infected with Respiratory Syncytial Virus.* Viruses, 2020. **12**(10).

696 24. Welsh, S., et al., *Antitumor activity and pharmacodynamic properties of PX-478, an inhibitor*
697 *of hypoxia-inducible factor-1α.* Molecular Cancer Therapeutics, 2004. **3**(3): p. 233-244.

698 25. Palayoor, S.T., et al., *PX-478, an inhibitor of hypoxia-inducible factor-1α, enhances*
699 *radiosensitivity of prostate carcinoma cells.* International Journal of Cancer, 2008. **123**(10):
700 p. 2430-2437.

701 26. Villa-Roel, N., et al., *Hypoxia inducible factor 1α inhibitor PX-478 reduces atherosclerosis in*
702 *mice.* Atherosclerosis, 2022. **344**: p. 20-30.

703 27. Sun, K., et al., *Selective Inhibition of Hypoxia-Inducible Factor 1α Ameliorates Adipose*
704 *Tissue Dysfunction.* Molecular and Cellular Biology, 2013. **33**(5): p. 904-917.

705 28. Ilegems, E., et al., *HIF-1a inhibitor PX-478 preserves pancreatic beta cell function in*
706 *diabetes.* Science Translational Medicine, 2022. **14**(638): p. eaba9112.

707 29. McGettrick, A.F. and L.A.J. O'Neill, *The Role of HIF in Immunity and Inflammation.* Cell
708 Metab, 2020. **32**(4): p. 524-536.

709 30. Bhat, R., M.A. Farrag, and F.N. Almajhdi, *Double-edged role of natural killer cells during*
710 *RSV infection.* Int Rev Immunol, 2020. **39**(5): p. 233-244.

711 31. Bergeron, H.C. and R.A. Tripp, *Immunopathology of RSV: An Updated Review.* Viruses,
712 2021. **13**(12): p. 2478.

713 32. Luckheeram, R.V., et al., *$CD4^+$T cells: differentiation and functions.* Clin Dev Immunol,
714 2012. **2012**: p. 925135.

715 33. Schmidt, M.E. and S.M. Varga, *Cytokines and CD8 T cell immunity during respiratory*
716 *syncytial virus infection.* Cytokine, 2020. **133**: p. 154481.

717 34. Currie, S.M., et al., *The human cathelicidin LL-37 has antiviral activity against respiratory*
718 *syncytial virus.* PLoS One, 2013. **8**(8): p. e73659.

719 35. Dabo, A.J., et al., *Matrix Metalloproteinase 9 Exerts Antiviral Activity against Respiratory*
720 *Syncytial Virus.* PLoS One, 2015. **10**(8): p. e0135970.

721 36. Hartshorn, K.L., et al., *Innate defense against influenza A virus: activity of human neutrophil*
722 *defensins and interactions of defensins with surfactant protein D.* J Immunol, 2006. **176**(11):
723 p. 6962-72.

724 37. Dos Ramos Almeida, C.J.L., et al., *Neutrophil Virucidal Activity Against SARS-CoV-2 Is*
725 *Mediated by Neutrophil Extracellular Traps.* J Infect Dis, 2024. **229**(5): p. 1352-1365.

726 38. Hsu, T.-S., et al., *HIF-2α is indispensable for regulatory T cell function.* Nature
727 Communications, 2020. **11**(1): p. 5005.

728 39. Ajouaou, Y., et al., *The oxygen sensor prolyl hydroxylase domain 2 regulates the in vivo*
729 *suppressive capacity of regulatory T cells.* eLife, 2022. **11**: p. e70555.

730 40. Bowlin, A., et al., *Hypoxia-Inducible Factor Signaling in Macrophages Promotes*
731 *Lymphangiogenesis in Leishmania major Infection.* Infect Immun, 2021. **89**(8): p. e0012421.

732 41. Czopik, A.K., et al., *HIF-2α-dependent induction of miR-29a restrains T(H)1 activity during*
733 *T cell dependent colitis.* Nat Commun, 2024. **15**(1): p. 8042.

734 42. Ahmad, T., et al., *Hypoxia response in asthma: differential modulation on inflammation and*
735 *epithelial injury.* Am J Respir Cell Mol Biol, 2012. **47**(1): p. 1-10.

736 43. Dewitz, C., et al., *Hypoxia-inducible factor-1α inhibition modulates airway*
737 *hyperresponsiveness and nitric oxide levels in a BALB/c mouse model of asthma.* Clinical
738 Immunology, 2017. **176**: p. 94-99.

739 44. Pan, S., S. Conaway, Jr., and D.A. Deshpande, *Mitochondrial regulation of airway smooth*
740 *muscle functions in health and pulmonary diseases.* Arch Biochem Biophys, 2019. **663**: p.
741 109-119.

742 45. Bartman, C.M., et al., *Cellular clocks in hyperoxia effects on [Ca2+]i regulation in*
743 *developing human airway smooth muscle.* American Journal of Physiology-Lung Cellular and
744 Molecular Physiology, 2021. **320**(3): p. L451-L466.

745 46. Evans, C.E., *Hypoxia-Inducible Factor Signaling in Inflammatory Lung Injury and Repair.*
746 Cells, 2022. **11**(2).

747 47. Rodriguez, D., et al., *Hypoxia Pathway Proteins and Their Impact on the Blood Vasculature.*
748 International Journal of Molecular Sciences, 2021. **22**(17): p. 9191.

749 48. Tian, M., et al., *HIF-1α promotes SARS-CoV-2 infection and aggravates inflammatory*
750 *responses to COVID-19.* Signal Transduct Target Ther, 2021. **6**(1): p. 308.

751 49. Wing, P.A.C., et al., *Hypoxic and pharmacological activation of HIF inhibits SARS-CoV-2*
752 *infection of lung epithelial cells.* Cell Reports, 2021. **35**(3): p. 109020.

753 50. Wing, P.A.C., et al., *Hypoxia inducible factors regulate infectious SARS-CoV-2, epithelial*
754 *damage and respiratory symptoms in a hamster COVID-19 model.* PLoS Pathog, 2022. **18**(9):
755 p. e1010807.

756 51. Ren, L., et al., *Influenza A virus (H1N1) triggers a hypoxic response by stabilizing hypoxia-*
757 *inducible factor-1α via inhibition of proteasome.* Virology, 2019. **530**: p. 51-58.

758 52. Ren, L., et al., *Influenza A Virus (H1N1) Infection Induces Glycolysis to Facilitate Viral*
759 *Replication.* Virol Sin, 2021. **36**(6): p. 1532-1542.

760 53. Zhao, C., et al., *Deficiency of HIF-1α enhances influenza A virus replication by promoting*
761 *autophagy in alveolar type II epithelial cells.* Emerging microbes & infections, 2020. **9**(1): p.
762 691-706.

763